Architecture for a Future C-band/L-band GNSS Mission

Part 2: Signal Considerations and Related User Terminal Aspects

JOSE-ANGEL AVILA-RODRIGUEZ
JONG-HOON WON
STEFAN WALLNER
MARCO ANGHILERI
BERND EISSFELLER
BERTHOLD LANKL
TORBEN SCHÜLER
UNIVERSITY FAF MUNICH

OLIVER BALBACH
IFEN GMBH

ANDREAS SCHMITZ-PEIFFER
JEAN-JACQUES FLOCH
LARS STOPFKUCHEN
DIRK FELBACH
EADS ASTRIUM

ANTONIO FERNANDEZ
DEIMOS SPACE

ROLF JORGENSEN
TICRA

ENRICO COLZI
ESA-ESTEC/VEGA IN SPACE

AUTHORS NOTE: *IT IS HIGHLY REMARKED THAT THIS COLUMN IS BASED UPON A C-BAND GNSS STUDY BEING CONDUCTED WITHIN THE EUROPEAN SPACE AGENCY (ESA) GNSS EVOLUTION PROGRAM. PLEASE NOTE THAT THE VIEWS EXPRESSED IN THE FOLLOWING REFLECT SOLELY THE OPINIONS OF THE AUTHORS AND DO NOT REPRESENT THOSE OF ESA.*

This column continues an exploration of possible use of the C-band radio frequency for GNSS navigation. Part 2 focuses on C-band signal design in the context of non-interference with other services in nearby RF bands, as well as user equipment design and performance.

The radio navigation satellite service (RNSS) portion of the radio frequency (RF) spectrum is already overcrowded, and the bands suitable for new uses are very limited. This is especially true for the E1/L1 band occupied today by GPS and Galileo.

In addition, Japan's quasi-zenith satellite system (QZSS) and potentially also Compass and GLONASS will be transmitting navigation signals in this frequency band. But E1/L1 is not the only case. Even those RF bands that are not being used yet will certainly be shared by many systems in the near future.

Thus, the search for unused frequency resources will almost certainly continue during the next years. The World Radio Communications Conference 2000 (WRC-2000) allocated the portion of C-band between 5010 and 5030 MHz for RNSS space-to-Earth applications. The general idea was to provide access to a frequency band that is not yet overloaded by other signal sources and, consequently, not so susceptible to interfering signals as guided by International Telecommunications Union (ITU) regulations.

Navigation in C-band presents both advantages and disadvantages, the most important drawback being the higher free space losses due to the limitations on the higher signal frequency. An omnidirectional C-band antenna at 5 GHz will be 3.2 times smaller in the linear dimension than an equivalent L1-band antenna. (The latter signal has a 19-centimeter wavelength at 1.575 GHz compared to the wavelength of 6 centimeters at 5.015 GHz.)

Because of this wavelength-driven design factor, the area of the C-band antenna will be 10 times smaller than that of a standard L-band antenna. As a result, a C-band antenna receives only 1/10th the broadcast power of its L-band counterpart. (For details of relevant research, see the articles by M. Irsigler et alia and A. Schmitz-Peiffer et alia (2008) in the Additional Resources section near the end of this article.)

Another important factor is the increased signal attenuation of C-band signals due to foliage, heavy rain, or indoors, as well as other negative environmental effects on signal tracking. On the other hand, C-band exhibits much smaller ionospheric errors for standard single-frequency applications. The hope is that technological progress might balance some of the disadvantages from a long-term point of view, given that an actual application of C-band for RNSS is not foreseen before the year 2020.

We began our discussion in the previous column (May/June 2009, *Inside GNSS*) with an explanation of the scope of the C-band project, service analysis, satellite constellations, ground segment, satellite transmit signal power requirement, payload design, spacecraft accommodation, and end-to-end performance.

In this column we talk about the C-band signal design driven to respect the given constraints of other C-band services, and the C-band user terminal equipment design and performance analysis in the context of expected applications.

Additional discussion of the navigation message structure design and the related added value concerning the troposphere corrections (e.g., the combination of navigation data and numerical weather data from meteorological satellites), together with critical user-terminal technologies needed to prepare C-band for use in a future GNSS constellation, have been added to this digital and online version of the article.

C-Band Signals Considered

Based on a thorough trade-off analysis, the Service with Precision and Robustness (SPR-C) and the Public Regulated Service for C-band (PRS-C) have been identified for a future Galileo signal plan in C-band.

A quick look at this service definition reveals the main motivation for both services: 1) the SPR-C was to maximize the possible user communities under C-band, following the civil/public dual-use concept of satellite navigation; 2) the PRS-C was to provide selected users with the access to this service in order to fulfill high security requirements (e.g., anti-jamming and anti-spoofing).

As discussed in the first part of this series, the PRS-C consists of two small spot beams with approximately 1,500 kilometers of radius. Moreover, these two spot beams shall provide high geographic flexibility to point at any required area on earth.

In addition, use of C-band shall aim at mitigating problem areas of current L-band signals. In fact, the C-band Service Plan was designed to address the vulnerability of L-band in critical infrastructures by providing additional robustness in degraded RF situations. Moreover, the proliferation of GNSSs and lack of high precision signals that work on a single frequency have also been important drivers in the C-band study.

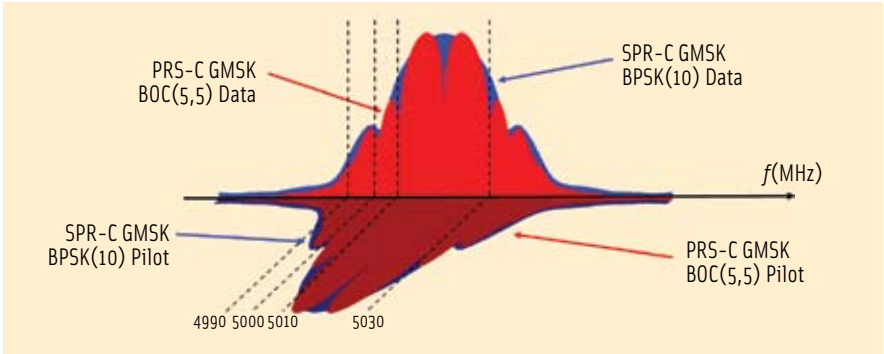

FIGURE 1 C-band GMSK Signal Plan

In order to design C-band signals the top-level requirements for both services were analyzed and established in terms of geometric dilution of precision (GDOP), availability, and continuity risk among other factors, and so on. In addition to this, the SPR-C requires authentication capability to provide robustness in terms of anti-spoofing while the PRS-C needs code-encryption capability to provide enhanced anti-spoofing performance. Both service signals should be spectrally decoupled from each other.

The C-band signal plan was optimized for maximum occupied bandwidth and spectral separation between the two provided services. In consequence, the signals presented next must be interpreted as an envelope of solutions in the sense that derived alternative signals with lower chip-rate and lower sub-carrier frequencies would also fulfill the criteria for compatibility with nearby C-band services. These are namely the radio-astronomy service (RA), the microwave landing system (MLS) service (MLS), and the Galileo up-link (UL) service.

Figure 1 shows the spectrum of the selected signal plan for C-band RNSS signals relying on the Gaussian minimum shift keying (GMSK) modulation. This scheme was found to satisfactorily accomplish the stringent requirements on spectrum confinement to ensure compatibility with adjoining C-band services. **Table 1** summarizes the parameters of the selected signal plan for the C-band.

Note that both the SPR-C and PRS-C services provide a data and a pilot channel.

Compatibility of C-Band Signals

Compatibility is the fundamental aspect in the design of any navigational signal. Indeed, this criterion was assigned higher priority than other characteristics such as navigation performance. As briefly mentioned earlier, the signal plan in the C-band must be compatible with:

- radio-astronomy (RA) band between 4990 and 5000 MHz
- microwave landing system (MLS) between 5030 and 5150 MHz
- Galileo uplink receiver (ULR) between 5000 and 5010 MHz

We will first describe our assumptions in calculating the potential for C-band interference and describe the GMSK signal in greater detail before reporting the results of our compatibility analysis.

Radio-Astronomy. RA compatibility is assured according to International Telecommunication Union (ITU) regulations if the power flux density (PFD) of the C-band downlink signals is not higher than a threshold value that is a function of the number of simultaneous satellites within the very narrow beam of an RA telescope.

In our analysis we assumed that a maximum number of 10 C-band satellites could be seen at any time by any RA antenna on the ground and that all the signals coming from these satellites have the same power at the surface of the Earth. Given that the antenna beam of

Frequency Band	C-band, 5010 to 5030 MHz			
Service	SPR-C		PRS-C	
Channel	Data	Pilot	Data	Pilot
Signal type	BPSK(10)	BPSK(10)	BOC(5,5)	BOC(5,5)
Modulation	GMSK $BT_c = 0.3$	GMSK $BT_c = 0.3$	GMSK $BT_c = 0.3$	GMSK $BT_c = 0.3$
Symbol rate	50 sps	N/A	--	N/A
Maximum code length	51,150	k*51,150	--	--

TABLE 1. Parameters of considered C-band signals

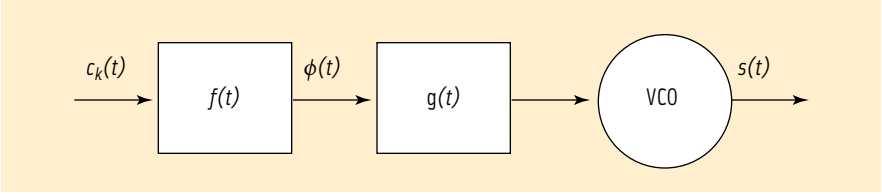

FIGURE 2 GMSK generation scheme

the RA receivers is very narrow, no more than a few satellites are expected to be in sight at the same time in the worst case. Furthermore, in the PFD computation we assumed atmospheric losses of 0.5 dB in signal power and included the whole 10-MHz RA bandwidth in measuring the combined C-band PFD at the surface of the Earth.

Moreover, we included both the spectrum of the SPR-C and the PRS-C in our calculations, although the SPR-C has global coverage and the PRS-C spot beams limit their operation to small regional "footprints." Again, as one can imagine, this is very much a worst-case scenario because most of the time only the SPR-C will potentially affect compatibility with the RA band, and the impact of PRS-C signals will be restricted to local areas.

Furthermore, to ensure compatibility with the RA band, we calculated the aggregate power flux density (PFD) of the downlink C-band signals of all satellites under consideration within the RA band such that the maximum PFD shall not exceed the corresponding threshold value.

Microwave Landing System. In order not to cause harmful interference to the MLS operating above 5030 MHz, the aggregate power flux-density produced at the earth's surface in the band 5030–5150 MHz by all the space stations within any RNSS system (space-to-Earth) operating in the band 5000–5030 MHz shall not exceed a threshold value of -124.5 dBW/m^2 in any 150 kHz band.

It has turned out that the most stringent constraint on out-of-band (OOB) emissions actually comes from the RA band, while the MLS band seems to be less problematic. Accordingly, the compatibility with the services on the right (upper) part of the C-band spectrum has proven to be relatively easy to accomplish while the left (lower) part raises serious concerns.

Galileo Uplink Receiver. In order to measure the maximum tolerable received power that can come from the C-band downlink signals without affecting the correct functioning of the uplink receiver in the satellite, the minimum C/N_0 for data demodulation shall not be lower than a certain threshold required to achieve a specified performance in terms of bit error rate (BER).

This criterion basically relies on the computation of the spectral separation coefficient (SSC) between the OOB emissions of the proposed downlink services and the C-band uplink. In fact, the underlying idea is to measure the increase of the equivalent noise that the uplink receiver will observe when the downlink signals leak into the receiver as additional noise.

To compute the quantitative available margin we first need to compute the C/N_0 of the uplink receiver in the absence of interference from downlink signals. The contribution of the equivalent noise due to the interfering C-band downlink signals, including output multiplexer (OMUX) filtering, basically depends on the SSC between the downlink signals and the uplink signals of the Galileo Uplink receiver as well as on the power of the downlink signals as seen by the uplink receiver.

In addition to these considerations, in order to compute the power of the downlink signals that leaks into the uplink receiver, we need to consider the antenna decoupling between them. Note that the interference scenario between the downlink signals and the uplink receiver does not correspond to a far field case. From the antenna point of view, both the uplink receiver antenna as well as the downlink transmission antenna are located very close to each other and, thus, near-field approximations have to be taken into account.

Given this situation, the common solution of using a combined transmit/receiver antenna will not work and, instead, we must consider an antenna coupling approach. In our simulations, a value of -110 dB was calculated based on the antenna design, and distance and power flux density. Additionally, approximately 4.4 dB were assumed for the antenna losses in terms of negative gain of the uplink receiver antenna.

Gaussian MSK (GMSK)

GMSK is a special case of continuous phase frequency-shift keying (CP-FSK) that employs Gaussian filtered frequency pulses to smooth the transitions from one point to the next in the signal status constellation while minimum shift keying (MSK) is obtained directly from the rectangular shape of frequency pulses.

The CP-FSK signal can be modelled mathematically after modulating it onto the RF carrier as follows:

$$s_n(t) = \sqrt{2P}\cos(2\pi f_c t + \phi_n(t) + \phi_0) \quad (1)$$

where P is the power of the carrier, f_c is the center frequency, $\phi_n(t)$ is the phase of the modulated carrier, and ϕ_o is the constant phase offset.

Figure 2 presents a simplified model to generate GMSK signals.

In the case of GMSK, the phase does not evolve linearly in the time domain.

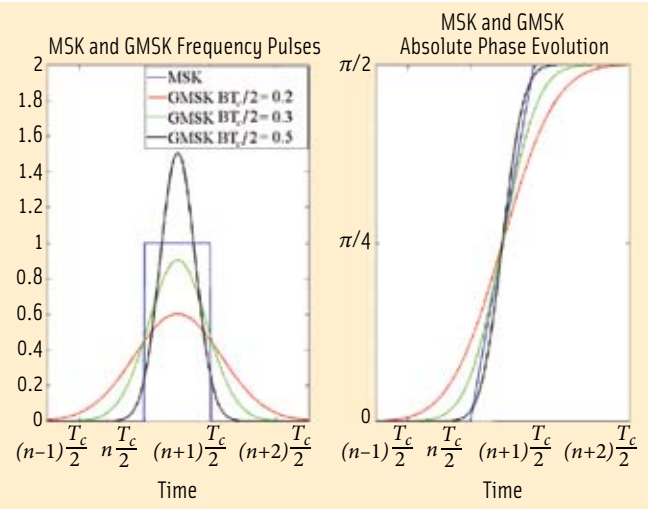

FIGURE 3 Comparison between frequency pulses and phase pulses of MSK and GMSK

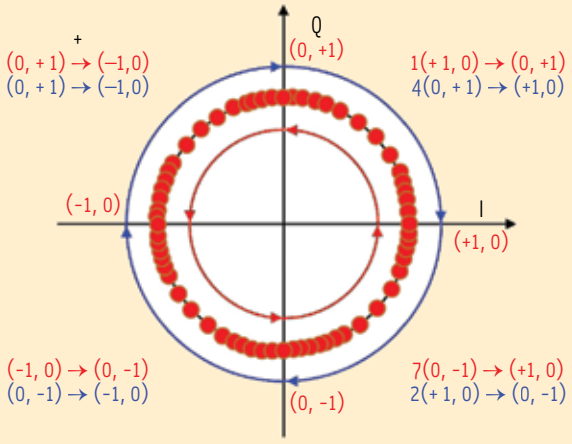

FIGURE 4 Phase evolution of GMSK

The evolution of the frequency over time adopts the following expression:

$$f(t)=\sum_k c_k(t)p\left(t-kT_c^{complex}\right) \quad (2)$$

where $T_c^{complex}$ represents the time duration of complex source codes. We need to distinguish the individual bits or chips (to be transmitted in the I-phase or respectively in the Q-phase) from the complex symbols that the I- and Q-chips constitute together. These chips result indeed from multiplexing the signal. This means in other words that whenever we refer to T_c, this will actually represent the chip duration of an individual PRN-code chip sent either on the I-channel or on the Q-channel. Consequently the duration of a I- and Q-chip tuple corresponds to a period of $T_c^{complex}=0.5T_c^{real}=0.5T_c$.

Note that the single frequency pulse $p(t)$ is no longer rectangular but can be expressed as the convolution of a rectangular pulse $p(t)$ with the Gaussian filter impulse response $g(t)$:

$$p(t)=h(t)\otimes g(t)=\int_{-\infty}^{\infty} g(\tau)h(t-\tau)d\tau \quad (3)$$

with

$$h_n(t)=\begin{cases}\dfrac{1}{2T_c^{complex}} & nT_c^{complex}\le t\le (n+1)T_c^{complex},\\ 0 & \text{elsewhere}\end{cases} \quad (4)$$

The Gaussian filter $g(t)$ adopts the following form in the time domain

$$g(t)=\frac{1}{\sigma T_c^{complex}\sqrt{2\pi}}\exp\left(\frac{t^2}{2\sigma^2\left(T_c^{complex}\right)^2}\right) \quad (5)$$

where

$$\sigma=\frac{\sqrt{\ln(2)}}{2\pi\ BT_c^{complex}} \quad (6)$$

In the definition of σ above, the product $BT_c^{complex}$ is defined as the -3 dB bandwidth-symbol time (BT) product. The higher this value is, the cleaner will be the eye diagram of the signal, but the higher the OOB emissions will be. On the other hand, the lower the selected product $BT_c^{complex}$ is, the more power will be concentrated close to the center of the band, which is actually the objective. However, this comes at the cost of higher inter-chip-interference (ICI).

A typical value in communication applications is $BT_c^{complex}$=0.3, which is a good compromise between spectral efficiency and ISI. As an example, the mobile communication standard GSM is based on GMSK with $BT_c^{complex}$=0.3. It must be noted that inter-symbol-interference (ISI) is basically the same if ICI applies to chips and ISI to symbols.

The frequency pulses as well as the derived phase pulses for MSK and GMSK with different factors $BT_c^{complex}$ are shown in **Figure 3** for comparison.

As we can see from this figure, the frequency pulse of the GMSK with $BT_c^{complex}$ lasts over approximately three chips, resulting in controlled but non-desired ICI.

The phase diagram of GMSK is similar to that of the MSK modulation with the difference that the transition from one point of the constellation to another one is not realized at a constant linear rate but instead follows a Gaussian distribution. That is, GMSK begins with a slow velocity at the starting phase constellation point, speeds up, and then slows down again when approaching the final phase constellation point.

By doing this, we can ensure that, independent of the sampling point in the receiver, the probability of being near the constellation point of interest (widest point in the eye diagram) will be higher. This is clearly depicted in **Figure 4**. The density of points indicates that the state of the signal adopts this value with a higher probability.

The C-band study considered different values for the bandwidth-symbol time (BT) factor, with the solution $BT_c^{complex}$ = 0.3 actually being the most interesting due to its good compromise between spectral confinement and the ISI in the time domain. **Figure 5** shows the comparison in terms of power spectral densities (PSDs) between two GMSK signal plans. In the figure, we denote them as GMSK^1 (with $BT_c^{complex}$=0.3) and GMSK^2 (with $BT_c^{complex}$= 0.25), respectively.

As we can recognize, the difference between both options is minimal from the point of view of their spectrum. However, in the time domain GMSK^1 (with $BT_c^{complex}$= 0.3) is shown to be more favorable as outlined in Figure 3 and Figure 5.

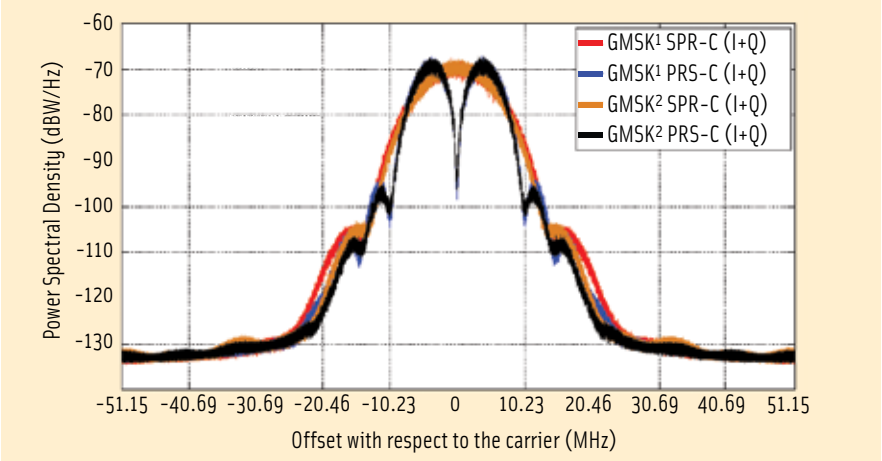

FIGURE 5 Comparison of GMSK signals for $BT_c^{complex}$ = 0.3 and with $BT_c^{complex}$ = 0.25

Compatibility of GMSK Signals

Next we will summarize the most important results on compatibility of the GMSK signals:

- **Compatibility with the radio astronomy:** the aggregate PFD of the composite SPR-C and PRS-C signal presents a value with which the RA constraints, as outlined in the previous page, are met satisfactory.
- **Compatibility with the uplink receiver:** as we have seen in previous sections, this is mainly driven by the SSC between the uplink and downlink signals of Galileo in C-band. Accordingly, we show in Table 2 the values of the SSC for each service separately. With the GMSK C-band signal plan, the effective C/N_0 required for data demodulation can be assured.
- **Compatibility with MLS:** as we already said, this is the least stringent constrain in the band. Indeed, the GMSK signal plan is well below the MLS PFD level of -124.5 dBW/m^2

It is important to note that, given the different directivity of the SPR-C and PRS-C antennas, the contribution of each service to the PFD on the ground will strongly depend on the final equivalent isotropic radiated power (EIRP). This was all taken into account in the calculations.

Payload Constraints

As we have seen in previous sections, the main constraint of C-band for navigation is the very small amount of bandwidth that is available, together with the very stringent requirements for compatibility with the nearby services. This is particularly difficult for the case of the uplink receiver, which is spectrally located directly on the left of the assigned downlink band. The simplest way to ensure compatibility would be to directly filter the signals after generation, using a steep raised cosine filter, for example.

Unfortunately, even though the signal might have been generated with a constant envelope, the desired constant envelope properties are lost after filtering. Furthermore, non-linear effects would appear during the high power amplification (HPA) unless pre-distortion filters or a linearized HPA are employed.

The final effect is a spectral regrowth of those side-lobes we had attenuated previously, consequently losing all the benefits of this intermediate filtering. This is important to keep in mind during the design because no matter how ideal our signal might appear regarding its spectrum, if we cannot guarantee that the envelope of the signals will remain constant after the power amplification (PA), all the efforts invested in reducing the side-lobes will be in vain (assuming the need to have a constant envelope to be a main driver).

Indeed, this was the main driver when the constant envelope continuous phase modulation (CECPM) was selected as ideal candidate to meet all the

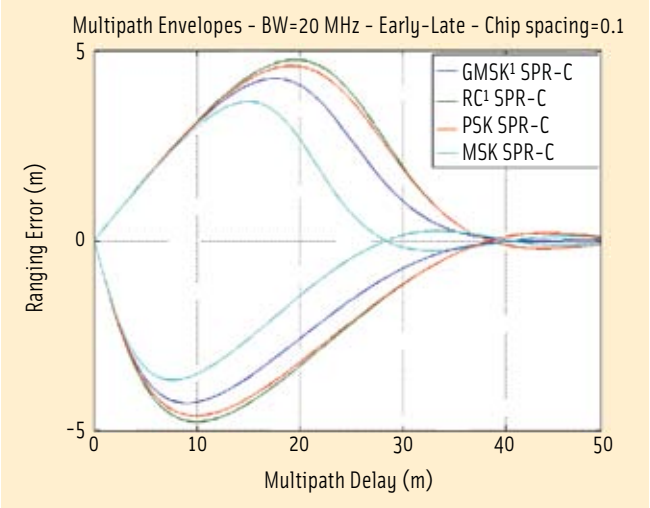

FIGURE 6 Multipath Envelopes of SPR-C signals

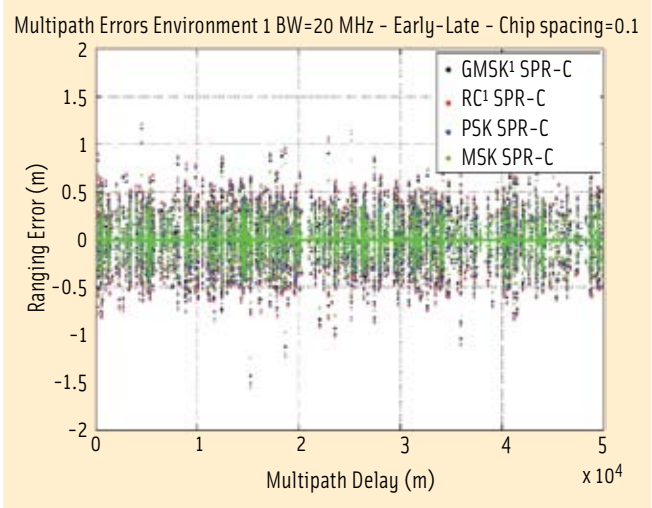

FIGURE 7 Multipath Error of SPR-C signals according to the LMS wideband model

requirements. The GMSK modulation is a constant envelope by definition, considerably simplifying all these aspects of the payload as a result. As discussed in further detail in Part 1, for the SPR-C a travelling wave tube amplifier (TWTA) was assumed, while for the PRS-C the selected amplifier is based on solid state amplifier (SSPA) technology.

GMSK Performance

We present in **Figures 6–9** the multipath performance of the proposed GMSK signals. In addition, other solutions considered in the definition of the C-band signal and service plan are also presented. We present first the results based on a single static multipath reflection with a signal to multipath ratio (SMR) of -6.5 dB.

Although SMR values of -3 dB are well established for L-band, the selection of an SMR value of -6.5 dB for C-band seems reasonable due to the higher ratio of diffuse reflections that can be expected for C-band compared to L-band. Later, the statistical wideband channel model for land mobile satellite systems (LMS) is employed.

As we can recognize, the best signal in terms of performance is MSK, followed by GMSK and SRC. MSK does not fulfill the compatibility requirements in the band and, accordingly, GMSK is shown to be the best option also in terms of performance. We need to keep in mind that, due to the tight constrains on C-band compatibility, any potential signal plan needs to first prove its compatibility with all the services around it. Only when the highest priority of compatibility is assured, can we concentrate on the proposed signals' performance.

For the simulations, a receiver bandwidth of 20 MHz was assumed. In addition, we used an early-minus-late discriminator with a spacing of 0.1 chips.

A quick look at the auto-correlation function (ACF) also reveals that, indeed, MSK has the sharpest slope around zero compared to the other assessed signals, which explains the superior performance of MSK in the previous figures. However, MSK could not demonstrate that it met the OOB emission requirements; thus, the best signal waveform among the compatible ones is GMSK. This coincides with the results shown in **Figure 10** and **Figure 11**.

To analyze the performance of the various signals in terms of their ICI effect on timing recovery and navigation data bit demodulation, the eye-diagram (and/or phase diagram) should be employed. We highly recommend that here the ICI or eye-diagram should be done at the chip level in order to show the effect of bandwidth-efficient methods (for example, GMSK, SRC, and so forth) compared to the phase shift keying (PSK).

In general the theory used in GMSK was derived for GMSK modulation of the data sequence, not the code sequence.

Signal Waveform	SSC [dB-Hz] between downlink and uplink
SPR-C GMSK BPSK(10)	-112.9304
PRS-C GMSK BOC(5,5)	-111.9697

TABLE 2. SSC between downlink and uplink

In the case of the GMSK with direct sequence spread spectrum (DSSS), ISI for data demodulation is not a problem because of the use of long correlation with a very short sampling time interval. Therefore, the eye-diagram for ISI in this case is unimportant.

Consequently, we proposed to introduce a new terminology of "ICI" (for inter-chip or code-interference). The name was already anticipated in previous discussion. Note that the proposed signal is the GMSK DSSS, which is different from the original GMSK with direct sequence frequency hopping (DSFH) that is widely used in GSM.

Figure 12 illustrates the eye-diagram summary of SPR-C signal for different cases of GMSK (BT=0.3 and 0.25) along three-chips intervals. Note that the eye-diagram of PSK should have a rectangular shape without any interference during the phase changing interval in absence of noise, i.e., the eyes are fully opened.

The GMSK BT=0.3 is slightly better than the GMSK BT=0.25, because the ICI of GMSK is inversely proportional to the bandwidth-symbol time (BT); so, a smaller BT provides a better performance in the sense of ICI, but we

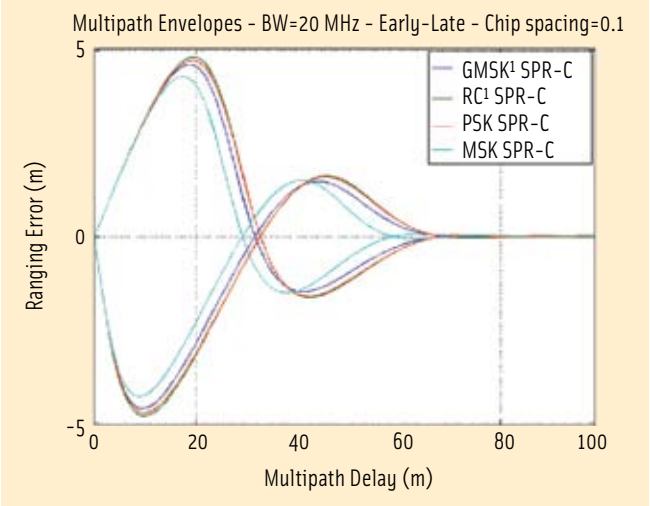

FIGURE 8 Multipath Envelopes of PRS-C signals

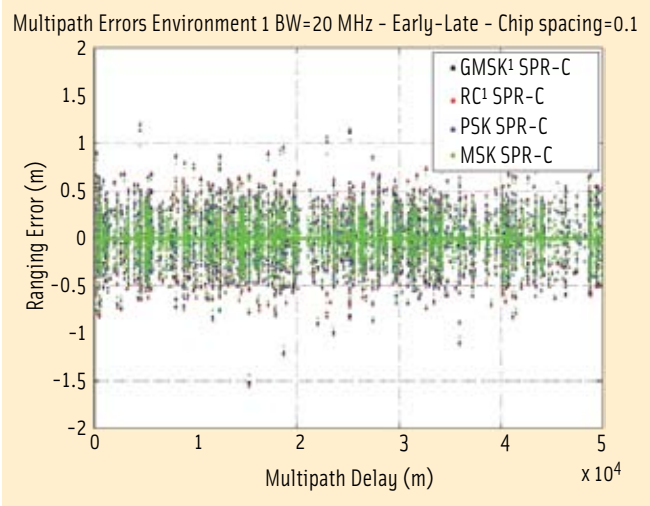

FIGURE 9 Multipath Error of PRS-C signals according to the LMS wideband model

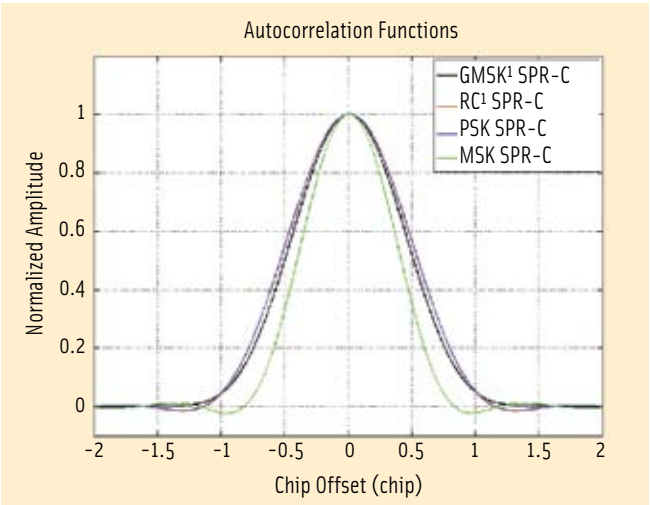

FIGURE 10 ACF of SPR-C signals

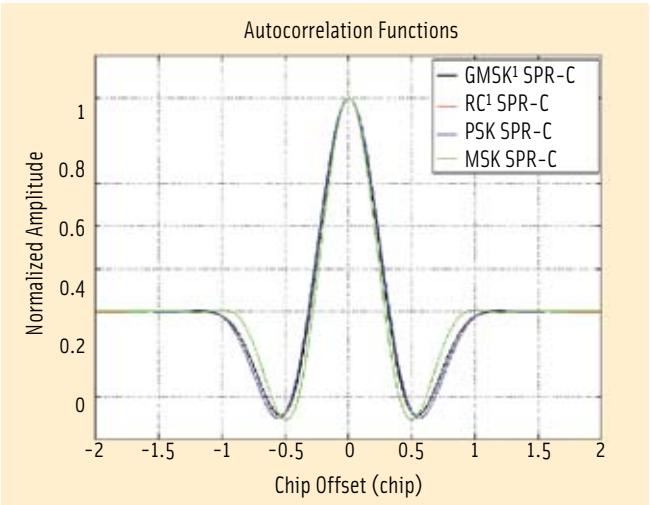

FIGURE 11 ACF of PRS-C signals

have to pay a price in spectral inefficiency. Nonetheless, the GMSK BT=0.3 still complies with the ITU regulations described earlier.

Overall User Terminal Architectures

The C-band signal was designed to make use of data and pilot channels. Using a pilot channel will provide a longer coherent integration, thereby producing less noisy range information.

For an extended discussion of C-band user terminal design concepts and performance analysis undertaken as part of the European GNSS Evolution program, see the three articles by J. H. Won et alia listed in the Additional Resources section.

The main identified core structure of SPR-C user terminals or receivers includes the following characteristics:

- A multi-bit ADC. This could be used for higher accuracy and is essentially required to achieve a more robust signal processing result when employing GMSK in a receiver.
- A data authentication module should be used for commercial services that are, of course, a core of the SPR-C service. This data authentication module provides the SPR-C user group with high-integrity information for safety-oriented applications such as aviation and maritime operations.
- SPR-C receivers would have various multi-frequency components (e.g., L-band) to provide precision positioning by efficient estimating of ionosphere errors, that is, dual-band user terminals (UTs).
- SPR-C UTs could have two different architectures depending on antenna designs — single antenna and array antenna systems. An SPR-C single-antenna system could use two omni-directional antennas for C- and L-band. (See **Figure 13**). The SPR-C array antenna system could incorporate an array antenna with digital beam forming control technology for C-band for more high-accuracy and robust precision services and an omni-directional antenna for L-band. The array antenna system has an amplitude and phase adjustment functional block in which inputs are output from an ADC bank in an RF chain. In order to control this amplitude and phase adjustment block, a navigation processor generates a command to control the digital beam-forming based on the receiver's heading and pitch angle information.

The main elements identified for the PRS-C UTs' core structure include:

- A decryption code generator for security access.
- Also, PRS-C UTs could have two different architectures depending on antenna systems: single antenna system and array antenna system: 1) For a single antenna system, an

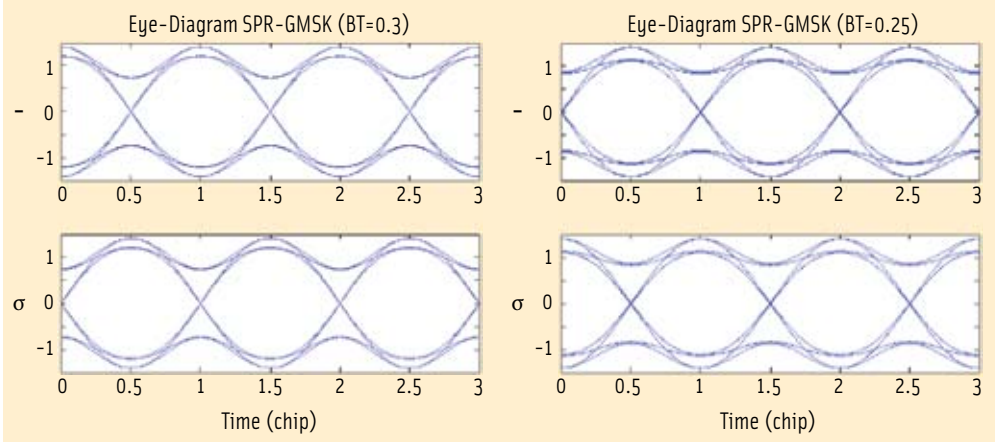

FIGURE 12 Eye diagram summary of SPR-C signal

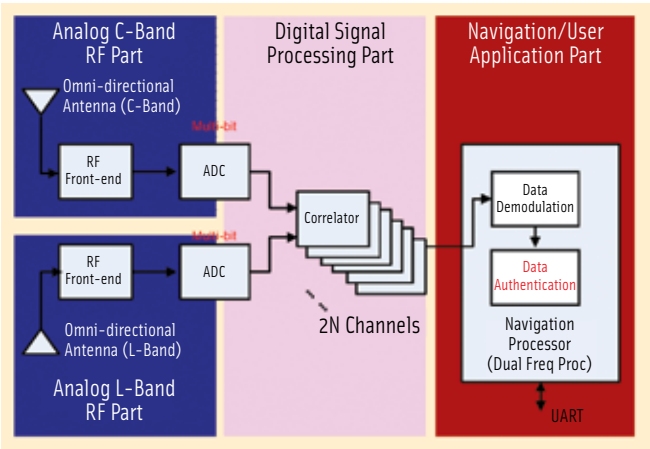

FIGURE 13 Schematic view on SPR-C UT architecture (single antenna system)

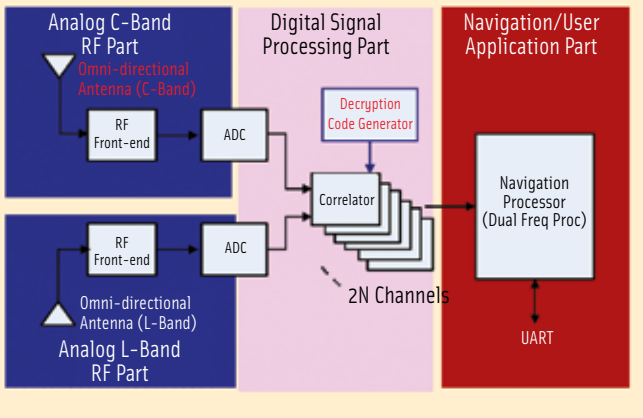

FIGURE 14 Schematic view on PRS-C UT architecture with single antenna system

omni-directional antenna should be also available to the C-band RF part for cost effective governmental user group, such as military handheld users (**Figure 14**); and 2) For an array antenna system, one array antenna with digital beam forming control technology for C-band should be available to C-band RF part for a level of additional anti-jamming margin to user terminals that require a higher anti-jamming capability. The array antenna system of PRS-C has the same control logic with the SPR-C array antenna system.

- Two antenna-driven architectures: a cost-effective, single-antenna C-band with omnidirectional design for governmental users, such as those needing military handhelds (Figure 16), and an array-antenna design with C-band digital beam-forming control technology for an additional level of anti-jamming capability and using the same control logic as the SPR-C array antenna system.

Signal-In-Space (SIS) Model

All GNSS signals-in-space (SIS) in the C-band (i.e., SPR-C and PRS-C) can be modeled as:

$$s(t) = s_{SPR}(t) + s_{PRS}(t) \quad (7)$$
$$= I_{SPR}(t) + Q_{SPR}(t) + I_{PRS}(t) + Q_{PRS}(t)$$

with

$$I_{SPR}(t) = \sqrt{2P_{I,SPR}}\,\tilde{C}_{I,SPR}(t-\tau)\cos\left((\omega_0+\omega_d)t+\phi\right) \quad (8)$$

$$Q_{SPR}(t) = \sqrt{2P_{Q,SPR}}\,C_{Q,SPR}(t-\tau-T_c/2)\sin\left((\omega_0+\omega_d)t+\phi\right) \quad (9)$$

$$I_{PRS}(t) = \sqrt{2P_{I,PRS}}\,\tilde{C}_{I,PRS}(t-\tau)\cos\left((\omega_0+\omega_d)t+\phi\right) \quad (10)$$

$$Q_{PRS}(t) = \sqrt{2P_{Q,PRS}}\,C_{Q,PRS}(t-\tau-T_c/2)\sin\left((\omega_0+\omega_d)t+\phi\right) \quad (11)$$

where $s_{SPR}(t)$ and $s_{PRS}(t)$ are the SPR-C and PRS-C signal, respectively; $I(t)$ and $Q(t)$ are the output signals coming from the I and Q branches, respectively; P is the signal power (assuming: $P_{I,SPR} = P_{Q,SPR}$ and $P_{I,PRS} = P_{Q,PRS}$); ω_0 is the angular frequency in radians/second; ϕ is the carrier phase in radians, τ is the code delay in seconds, ω_d are the angular Doppler frequency in rad/sec, d is the data bit (±1), respectively; $\tilde{C}_{I,SPR}$ is the shaped pulse of SPR-C PRN code in the I-channel multiplied by a subchip that already accounts for the data bit (i.e., a data channel), $C_{Q,SPR}$ is the shaped pulse of SPR-C PRN code in the Q-channel (i.e., pilot channel), $\tilde{C}_{I,PRS}$ is the shaped pulse of PRS-C PRN code in the I-channel multiplied by a subchip considering data bit (i.e, data channel), $C_{Q,SPR}$ is the shaped pulse of PRS-C PRN code in the Q-channel multiplied by a subchip (i.e, pilot), and T_c represents the code chip duration of each service signal in seconds.

We should emphasize that the use of $\tilde{C}$, that is a shaped-pulse code multiplied by a navigation data bit, is mainly for GMSK signals due to its continuous phase modulation property.

Note that the additional half-chip ($T_c/2$) code delay in the Q-channel comes from the "offset" in offset QPSK (OQPSK) to restrict an instant phase change within ±90 degrees, thereby reducing the spectral leakage of the intended signals as much as possible. If we omit the terms $T_c/2$ from the preceding equation — that is, with no delay between I and Q — the signal model becomes a generic balanced QPSK.

Let us turn our attention now to the models of the received signals. These models will then be used in the receiver design. Moreover, it must be noted that for the GMSK data channel, the received signal model does not need to have $\tilde{C}$ because the correlation between the data-modulated shaped pulse code ($\tilde{C}$) and the original shaped pulse code (C) that should be locally generated in a receiver would be done in a noncoherent way; so, the resulting correlation function has the same shape, and the polarity represents navigation data bit.

- SPR-GMSK-QPSK(10)

$$s_{SPR}(t) = I_{SPR}(t) + Q_{SPR}(t) \quad (12)$$
$$= \sqrt{2P_{I,SPR}}\,d_{SPR}(t-\tau)C_{I-GMSK,SPR}(t-\tau)\cos\left((\omega_0+\omega_d)t+\phi\right)$$
$$+\sqrt{2P_{Q,SPR}}\,C_{Q-GMSK,SPR}(t-\tau-T_c/2)\sin\left((\omega_0+\omega_d)t+\phi\right)$$

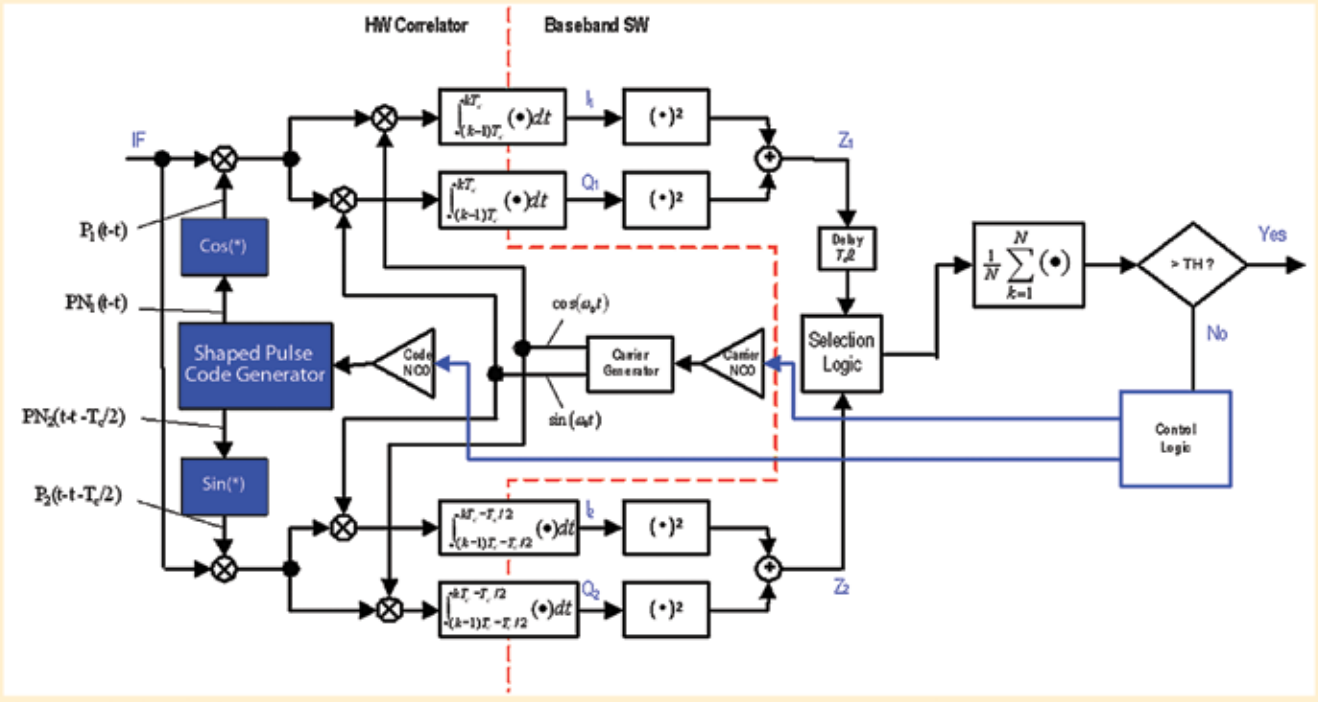

FIGURE 15 Block diagram of signal acquisition system for shaped-pulse OQPSK

- PRS-GMSK-QBOC(5,5)

$$s_{PRS}(t) = I_{PRS}(t) + Q_{PRS}(t) \quad (13)$$
$$= \sqrt{2P_{I,PRS}}\, d_{PRS}(t-\tau) C_{I\text{-}GMSK,PRS}(t-\tau)\cos\left((\omega_0+\omega_d)t+\phi\right)$$
$$+\sqrt{2P_{Q,PRS}}\, C_{Q-GMSK,PRS}(t-\tau-T_c/2)\sin\left((\omega_0+\omega_d)t+\phi\right)$$

Signal Acquisition

Figure 15 illustrates the proposed acquisition system block diagram for OQPSK DSSS. Note in the figure that the delays in the integrators are set to $T_c/2$ seconds, and the upper code branch is delayed by $T_c/2$ seconds.

The acquisition system consists of two BPSK acquisition detectors that produce the sum of I^2+Q^2 in a signal branch for the first SS code. This is added to the sum of I^2+Q^2 in the other signal branch for the second SS code in order to drive the non-coherent integration.

The block diagram contains a selection logic that combines the I and Q branches or selects one of them (representing combined data/pilot or pilot-only processing, respectively). This is because the I and Q codes of QPSK are synchronized to each other, and we need to search a given code-search range for I or Q that is the same as in the case of BPSK signals.

The only price that we have to pay in this case is a doubling of hardware resources (i.e., correlators), but we will have an important three-decibel gain in terms of C/N_0.

Table 3 shows the required processing power ratios that could be supported by the processing power anticipated to be available by 2020 and later. These power ratios are needed to fulfill a cold-start mean acquisition time (MAT) requirement with a sufficient C/N_0 (e.g., 40 dB-Hz) and a small false alarm–penalty time coefficient.

The table incorporates pessimistic, moderate, and optimistic assumptions on the increased processing capabilities with respect to the current available processing power, considering by factors of 10, 100, and 1000, respectively. Here we assumed that Moore's rule — a doubling of processing power every 18 months. The evolution of the processing power compared to the currently available processing power is assumed to be "140" because the maximum processing performance measured in teraflops/second is expected to rise from around 0.5 to 73 teraflops/second on a single chip by the year 2020+.

We used a "Hot Start Time" requirement in order not to be affected by the design of navigation data structure.

The cells with a ratio larger than "1" means that the expected signal processing power at 2020+ may not be sufficient to meet the acquisition time requirement. For example, with only a 100-fold increase in processing power from current levels (e.g., 25 multi-correlators and four times the sequential processing per channel), the processing-power figure for the SPR-C signal is on the order of 10-1 and fulfills the requirement, while the PRS-C needs still more signal processing capabilities.

Nevertheless, we need a processing power redundancy of a parallel operation of correlators for fast time to first fix (TTFF) and as high sensitivity as possible. Even with today's advanced technology, the future of the signal acquisition in C-band is in some sense bright.

In order to analyze the effect of GMSK on signal acquisition, we subtract the acquisition function of the unfiltered quadrature phase skip keying (QPSK) and quadrature binary offset carrier (QBOC) cases from the intended modulation cases. **Figure 16** illustrates the difference between normalized autocorrelations of GMSK and the unfiltered rectangular code case.

	System	Signal	Processing Power N_{proc}			Acquisition Time (Requirement)	Ratio compared to L2-band
			10x140	100x140	1000x140		
Low-end civil users	GPS	L1CA	$4x10^{-4}$	$4x10^{-5}$	$4x10^{-6}$	< 45 s (cold start)	-
High-end civil users	GPS	L2C	$1.017x10^{-1}$	$1.017x10^{-2}$	$1.017x10^{-3}$	< 30 s (hot start)	1
	GPS	L2P(Y)	$2.034x10^{0}$	$2.034x10^{-1}$	$2.034x10^{-2}$		20
	Galileo	E6-B,C	$1.070x10^{0}$	$1.070x10^{-1}$	$1.070x10^{-2}$		10
	SPR-C	QPSK(10)	$8.420x10^{0}$	$8.420x10^{-1}$	$8.420x10^{-2}$		80
High-end military (or governmental) users	GPS	L2M	$4.557x10^{1}$	$4.557x10^{0}$	$4.557x10^{-1}$	< 10 s (hot start)	1
	Galileo	E6-A	$4.661x10^{1}$	$4.661x10^{0}$	$4.661x10^{-1}$		1.02
	PRS-C	BOC(5,5)	$9.322x10^{1}$	$9.322x10^{0}$	$9.322x10^{-1}$		2.06

TABLE 3. Required processing power ratio at 2020+ for acquisition of GNSS signals

In those areas of the figure where the correlation value of GMSK is larger than that of the unfiltered rectangular code, acquisition is not a matter of concern; but the opposite case, i.e., when the correlation value of GMSK is smaller than that of unfiltered rectangular code, could pose a problem if the correlation value is smaller than the predefined acquisition threshold.

The latter situation forces us to reduce the code bin size to cover this smaller region, or to carefully choose the predefined threshold value, which is controlled by setting the detection and false-alarm probabilities. However, the analysis here was based on the unfiltered QPSK or QBOC cases. Therefore, if we consider a more realistic case, e.g., a band-limited QPSK or QBOC, the result might be more similar to that of GMSK.

Note that, for the proposed bandwidth-efficient modulation schemes, the only thing that needs to be modified in the signal-processing functional blocks of today's GPS/Galileo receivers (which are based on the PSK modulation scheme), is the correlator functional block. That is, if we replace the binary code PRN (or BOC) generator of a GPS/Galileo receiver with a code generator that creates the shaped-pulse codes proposed for SPR-C and PRS-C, we can easily implement a GMSK-based navigation receiver.

Signal Tracking

As with the signal acquisition scheme, a code- and carrier-tracking system for OQPSK DSSS signals was proposed consisting of two BPSK tracking blocks.

The main differences from the current BPSK-type Galileo receiver's signal tracking are 1) the shaped pulse code generator, 2) QPSK-type receiver, and 3) a block with an algorithm that combines the carrier and code to deal with a QPSK signal.

Figure 17 shows the whole non-coherent phase-lock-loop (PLL) noise jitters of SPR-C and PRS-C signals for a high-end user terminal (e.g., a vibration isolation–equipped user terminal). C/N_0 threshold to maintain PLL lock (i.e., the cross point of noise jitter line with the yellow threshold line) and tracking loop accuracy at high enough C/N_0 for noncoherent PLL can be read from the figure.

Due to the high dynamic stress requirement for the SPR-C, the 18-Hz noise bandwidth usually used for L1-band is shown to be not sufficient to accommodate dynamic ranges. The use of a narrow noise bandwidth in conjunction with a temperature-controlled crystal oscillator (TCXO) does not offer a solution because of the lack of margin for the signal tracking loop design. Increasing the noise bandwidth (e.g., 40 Hz) to give more design margin to the C-band would provide us with better accuracy, but we would then lose some amount of available C/N_0 in dB-Hz.

Accordingly, the best way to improve performance of both C/N_0 and accuracy is to use a rubidium oscillator as well as to increase the transmit signal power. The use of a rubidium oscillator will retain the C/N_0 ratio while providing a 4.0-degree tracking loop accuracy, which translates into a ranging accuracy of about 0.7 millimeter.

For PRS-C, we assumed a vibration specification of 10 g/s to test the vibration-induced phase noise jitter. The C-band

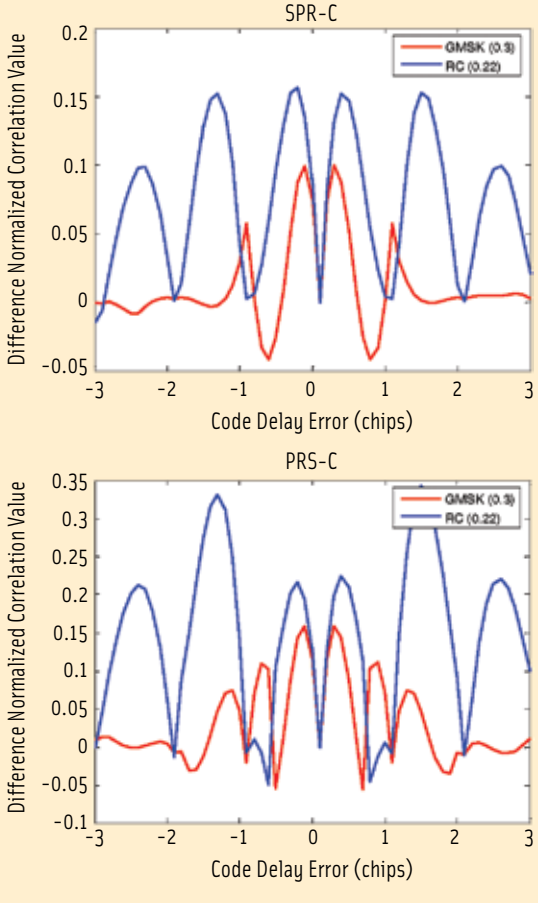

FIGURE 16 Difference of normalized autocorrelation functions: GMSK or SRC minus PSK

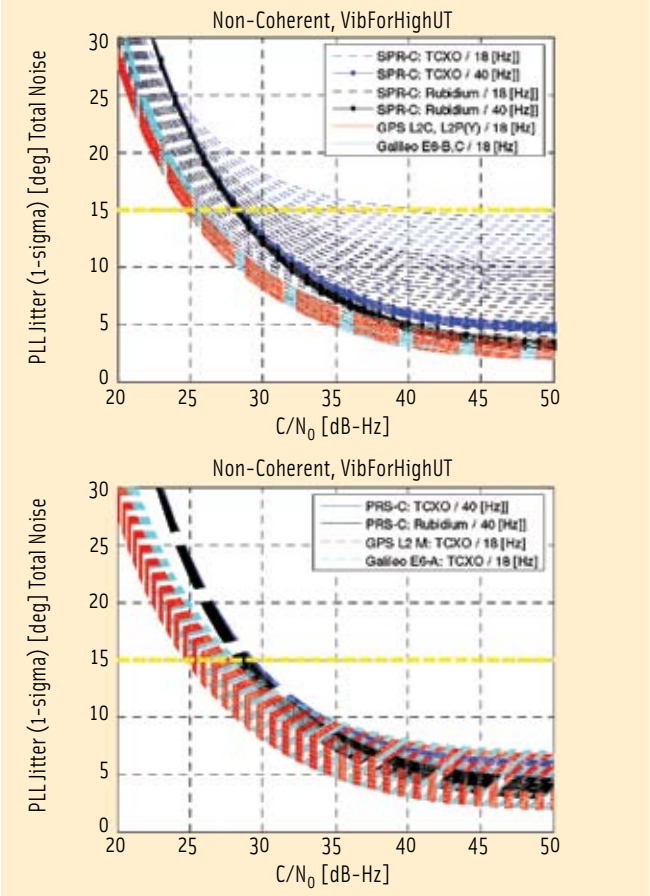

FIGURE 17 Non-coherent PLL total noise jitter for SPR-C (upper) and PRS-C (lower) in the case of vibration isolation–equipped user terminals

noise jitter, which is four times higher than that of L-band, would bring the C-band noise jitter line near to the threshold value (probability-of-false-alarm limit) even with a wide noise bandwidth and a high quality oscillator.

Since this would finally make the use of PRS-C impractical in a real-world environment, mounting the oscillator of a PRS-C receiver using well-designed vibration isolators is strongly recommended. A narrow noise bandwidth approach is not applicable to PRS-C because of its high dynamic requirement. Moreover, using a rubidium oscillator we can obtain a comparable performance as an L-band system in terms of C/N_0 and the tracking loop design margin.

A better oscillator also allows better C-band performance in terms of ranging accuracy, but not vibration-induced oscillator phase noise jitter. Without a well-designed vibration-isolation solution in the receiver, C-band UTs cannot accommodate a vibration environment even with a wide noise bandwidth. Therefore, vibration-isolation equipment is an essential design factor.

Before leaving this part of the discussion, we should point out that, given equivalent phase-tracking accuracy as an L1 (or L2) receiver, C-band ranging accuracy would be 3.2 times superior (or in the case of L2, four times higher) than that of L-band because the wave length of C-band is one-third that of L-band.

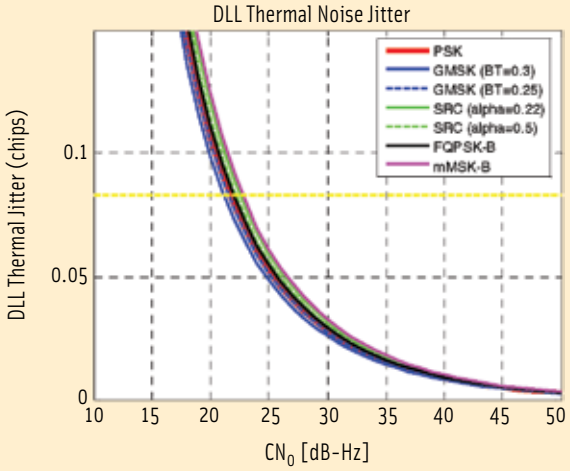

FIGURE 18 DLL thermal noise jitter for GMSK together with other solutions that were also investigated (0.5 delay spacing, B_{DLL}=40 Hz)

In order to analyze the effect of the GMSK design on UT tracking loops, we tested the delay-lock-loop (DLL) thermal noise jitter performance. **Figure 18** depicts the DLL jitter for several proposed signals. A 20-MHz bandwidth of receiver filtering was assumed for the case of filtered PSK, but not for other the other signals, because the bandwidth-efficient modulation scheme itself already includes the filtering effect.

Obviously, if we use band-limited signals, we lose a level of accuracy compared to the unfiltered ideal PSK. The accuracy of signal tracking (or, equivalently, ranging accuracy) depends on the sharpness of the correlation functions as seen in the UT. As we can observe, GMSK performs the best in terms of this criterion, followed by filtered PSK and then SRC.

Undoubtedly, an ideal unfiltered PSK approach would provide the best result but is not achievable in a real-world environment due to the use of band pass filters at the end of a GNSS satellite's RF chain and at the front-end of any type of typical receivers. Therefore, we conclude from the results shown in Figure 21 that GMSK provides a better accuracy than other methods. Moreover, we must also note that, at a sufficiently high C/N_0, all methods provide a similar level of accuracy.

Boundary Condition

Table 4 shows an SPR-C receiver's signal power budget under typical operating conditions. In the table, the worst and the best cases depend on satellite elevation angles. Key design parameters such as noise floor, antenna gain, correlation loss, noise figure, implementation loss and so on, were assumed in a reasonable way. The required C/N_0 at correlator (i.e., the C/N_0 threshold needed to maintain PLL lock) was obtained from a signal-tracking stability analysis by reading the crossing point of a PLL noise jitter line with the predefined threshold value.

The typical receiver operation C/N_0 region, where the noise jitter line is aligned almost horizontally and produces a reasonable accuracy of tracking results, was obtained at unshadowed environmental conditions where the satellite-receiver link loss

	Satellite at low elevation (10 deg) – worst case	Satellite at moderate elevation (40 deg)	Satellite at zenith (90 deg) – best case
Received signal power available to an isotropic antenna (C dBW)	-158.3	-156.3	-158.3
Typical patch antenna gain (G_R dBic) relative to isotropic antenna	-5	+0	+5
Receiver signal power available to typical patch antenna (C dBW)	-163.3	-156.3	-153.3
Noise floor (N_0 dBW)	-203 (nominal operation)		
LNA noise figure (N_f dB)	-2 (already included in No evaluation)		
Correlation loss (L_{corr} dB)	-1		
Implementation loss (L dB)	-1		
Precorrelation CNo (CNo dB-Hz) at correlator for nominal operation	37.7	44.7	47.7
Typical receiver operation region (dB-Hz)	37.7 ~ 47.7 dB-Hz (10 dB variation)		
Design margin (dB)	14.0±5 dB		
Threshold CN_0 (dB-Hz) for maintaining PLL lock	28.7 (TCXO@40Hz)		

TABLE 4 Receiver signal power budget at typical receiver operation region (SPR-C data)

only encompasses the free space loss, atmospheric loss, and receiver antenna polarization loss. Excluded from this calculation were other losses stemming from user environment–dependent power degradation factors, such as atmospheric attenuation in tropical region, tropospheric scintillation, foliage attenuation, interference and so on.

From the link budget analysis, we assumed the received signal power available to an isotropic antenna was -158.3 to -156.3 dBW, depending on elevation angles. Assuming the range of a typical patch antenna gain relative to an isotropic antenna, we calculated the receiver signal power available on a typical patch antenna to be -163.3 to -156.3 dBW. The threshold C/N_0 to maintain PLL lock in the case of data-only tracking channel is 28.7 dB-Hz from the extensive stability analysis on PLL. This fact means the C/N_0 design margins are 14±5 dB for the SPR-C.

C-band Navigation Message

Considering that two services (SPR-C and PRS-C) should be provided in the C-band, two corresponding variations of the C-band navigation message were proposed: PRS-C/NAV and SPR-C/NAV.

The main distinctions between these message types are due to the different transmission rate, resulting primarily from the ranging code design and from the different requirements of the two services in terms of the size of the area served and of the fields where they will find application.

As we will show in the following discussion, the structure of the C-band message contains a certain level of flexibility. Moreover, should the need arise to further differentiate the PRS-C/NAV from the SPR-C/NAV, a variable content subframe still leaves very large margins for further changes, especially in the arrangement of additional data or in the definition of specific, new message types.

Information to Be Transmitted. Identifying the minimum required amount of data to be transmitted was crucial for keeping the data transmission rate as low as possible, while still meeting the TTFF requirements.

The send-time information will be transmitted in the form of progressive counters related to special time intervals described a little later, while data to compute the satellite position and clock error consists of the traditional ephemeris and polynomial coefficients. This kind of satellite-specific information will be kept separate from the rest of the data.

In addition to this, there is all common information for providing a PNT service, such as GNSS system time conversion parameters, coordinated universal time (UTC) conversion parameters, ionospheric correction parameters, satellite health information, and almanac.

The C-band navigation message should contain additional data according to the requirements of the PRS-C and SPR-C services. Compared to the most traditional content, the following data will be included: fast clock differential corrections, digital signature for navigation message authentication (NMA), new encryption black key, and zenith hydrostatic and wet delay data for tropospheric corrections.

We should note that, in accordance with former decisions, no additional integrity information will be transmitted for both C-band services.

Message Structure. The overall message structure, common to the two message types, consists of a continuous stream of frames such as the one illustrated in Figure 19.

Each frame divides into three subframes, which are sent one after each other and present remarkable differences

FIGURE 19 Structure of the C-band message frame

concerning their function and content. As we will detail shortly, the error protection techniques employed for each message type will also be different. But first, let's take a closer look at the three subframes.

FCN Subframe. The first part of each frame is called the frame counter (FCN); it contains a progressive index, counting for the number of frames that have been transmitted since the last update of subframe 2, which essentially contains clock and ephemeris data (CED).

The FCN field is generated and transmitted simultaneously from all the satellites, and since the value of the counter will be the same, symbol combining over multiple paths will be possible. In this

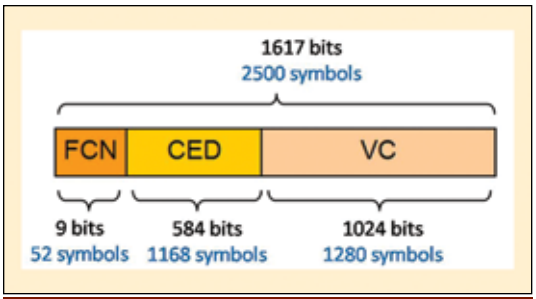

FIGURE 20 Total frame length of the C-band navigation message

way the demodulation threshold for the contained bits is decreased and the overall system gains in robustness.

The information contained in this part of the navigation message plays a very important role in determining the pseudoranges to the satellites: the receiver clock can be set just by reading this portion of the navigation message. Therefore, having such timing information available, especially in difficult environments such as urban canyons or even inside buildings, may represent a key feature for both SPR-C and PRS-C services. For this reason, as will be shown later, this part of the navigation message will be particularly protected against transmission errors.

CED Subframe. The clock and ephemeris data (CED) subframe contains the fundamental data that allows the user to compute the satellite position and time, providing precise ephemeris data as well as clock correction coefficients.

Other parameters present here are the week number and the interval counter in the current week, according to the system time related to the epoch when the current frame has been transmitted by the satellite.

The CED subframe presents validity duration of exactly two hours, after which new data is made available from the ground segment and transmitted to the users. With this guarantee, receivers can combine symbols over multiple frames in an effort to minimize the transmission errors.

Furthermore, the incoming data can be wiped-off by multiplying it with the previously stored symbols belonging to the same validity interval; thus, an additional pilot channel could be available for precise signal tracking.

VC Subframe. The last part of each frame is reserved for variable content (VC). This means that each frame could contain different data in this part of the navigation message.

The content of this subframe can be sent in an arbitrary sequence because the user can identify the following content looking at the message type identifier at the beginning of each VC subframe.

Figure 20 summarizes the amount of data forming the individual frames of the C-band navigation messages.

Value-Added Data. We turn now to a more extensive discussion about numerical weather and the encryption/authentication data.

Indeed, this data represents one of the most interesting points in the overall message design because of its importance in terms of the required service performance and because of the problematic aspect of the large amount of bits to be transmitted (especially concerning the wet and hydrostatic delay data for the SPR-C).

Clock Differential Corrections. Fast clock differential corrections are sent via the C-band messages, in order to meet the stringent accuracy requirements of the two C-band services.

These corrections are transmitted as variations to the polynomial coefficients that are used to compute the satellite clock error (δa_{f0} and δa_{f1}), together with an accuracy index and a five-bit field representing the PRN number of the satellite to which the clock corrections refer.

Zenith Wet and Hydrostatic Delay. For achieving high positioning performance, accurate tropospheric corrections should be carried out by the receivers. This kind of corrections can be computed based on two key parameters, namely the zenith wet and the hydrostatic delay.

The proposed model for the transmission of this tropospheric data requires 638 bits for each granule (block of 25 grid points). For the PRS-C service, sending two of these granules (each extends for 12 x 12 degrees) will be more than sufficient for covering the served area (1,500 kilometers in diameter). Different PRS-C/NAV messages will be transmitted on two separated signals, one for each individual area.

In case global coverage is required by the SPR-C, given a grid-resolution of 3 x 3 degrees, this information must be transmitted for 7,200 grid points, grouped into 288 granules.

However, because no maritime users are expected to require such high precision tropospheric corrections, the number of grid points can be significantly reduced (to around 100 granules) if the points over the oceans are excluded.

Furthermore, because the Arctic and Antarctic regions are very cold, the contribution of zenith wet and hydrostatic delays are expected to be very small. Therefore, the total number of granules to be transmitted could be reduced further.

Detailed Content of the Subframes. Figures 21–25 show the detailed content of each subframe and of three possible message types for the VC. As indicated earlier, data transmitted within the VC subframe can be arranged in any order according to specific requirements. Also, if additional content needs to be transmitted, numerous message types can be further defined and transmitted.

The three defined message types consist of a common type that is intended to be sent regularly, a second type containing the parameters to perform the navigation message authentication, and a third type allowing for the management of the encryption key, with a new "black" key being provided to users.

Error protection. We will now briefly explain the proposed techniques used to protect the C-band message from transmission errors.

Forward Error Correction. As introduced previously, the three subframes should be separately encoded, because of their different bit-error-rate (BER) performance requirement and because of the defined message structure.

Given the importance of the time parameter contained in the FCN sub-

frame, a strong high-redundancy block code is to be used to encode the 9 bits into 52 symbols.

For subframe 2 and 3 the use of low-density parity check (LDPC) codes is proposed: recent studies, mostly in the framework of the design of the new GPS L1C message, strongly recommend the use of codes for protecting the data.

Starting from the need for increasing the correction performance and approaching the Shannon capacity limit on the maximum amount of error-free digital data that can be transmitted, our study found that these codes outperform many other competitors in terms of correcting capability. Their performance is very close to that of turbo codes, but unlike the latter codes, LDPC codes have no intellectual property constraints on them, a factor that may be of great importance for their future use.

Table 5 presents the chosen coding schemes for the CED and VC subframes, together with some specific parameters.

Especially concerning the use of the 4/5 code, we should note the motivation that led to this choice did not come merely from the performance of this code. Obviously, lower coding rates could perform better, especially in more realistic channel models. However, when we had to make our design choice, we had to consider at the same time the requirement of having a data transmission rate that should be as low as possible, the big amount of data to be transmitted (weather model and fast clock corrections), and the need to guarantee a frame repetition time that could meet the TTFF requirements.

Therefore, a solution showing good BER performance while not introducing too much redundancy in the information to be transmitted would have been the best choice. In any case, quite a good margin remains for including further deterioration effects and still meeting the requirement of a BER of 10-5.

Block Interleaving. Another concept that turns out to be crucial and should be employed is block interleaving. The encoded navigation symbols are fed into a matrix row-by-row and then read column-by-column before being transmitted.

The receiver will then perform the inverse process before starting decoding the symbols. The advantage is that burst errors, which result from fading and shadowing, would be spread throughout a large portion of the message, facilitating the correction operated by the decoder.

Our design choice for the matrix is to have 48 rows and 51 columns. The following steps show the working principle of the interleaver and how it applies to the C-band navigation message: 1) subframe 2 and 3 are put together for the transmission, 2) they are then written into the matrix interleaver row-by-row, 3) the sequence to be transmitted is prepared reading the matrix content by columns, and 4) the interleaved sequence is transmitted.

Frame Duration and TTFF. Each complete frame is received within a given time: 25 seconds for PRS-C/NAV and 50 seconds for SPR-C/NAV.

Having available the satellite ephemeris and clock corrections, as well as the send time information (FCN) transmitted within each frame, the first pseudorange measurements can be carried out within the required TTFF (60 seconds for the SPR-C and 30 seconds for the PRS-C).

These considerations are based on the assumption that a direct acquisition, without referring to coarse satellite position computations from the almanac, is possible. This is true for most environments, while in the case of weak signals almanac data not older than one week should be available to the users (stored in the devices) for meeting the aforementioned TTFF requirements.

The following time would be required to retrieve both zenith wet and hydrostatic delay data and perform an accurate tropospheric correction. First, for the PRS-C, two granules for the interested area are transmitted within two frames

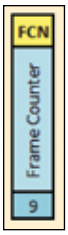

FIGURE 21 FCN subframe and number of required bits

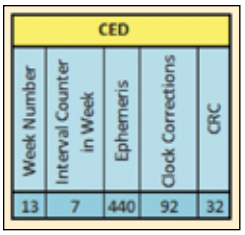

FIGURE 22 CED subframe and number of required bits

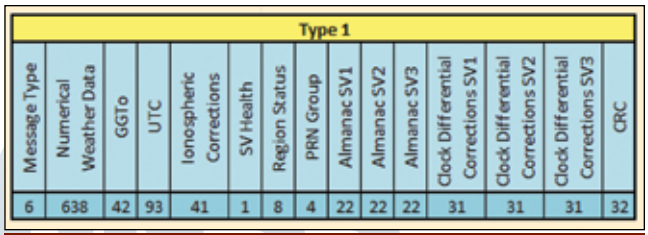

FIGURE 23 Type 1 message of the VC subframe and number of required bits

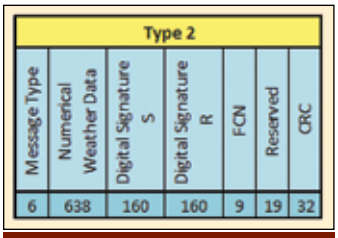

FIGURE 24 Type 2 message of the VC subframe and number of required bits

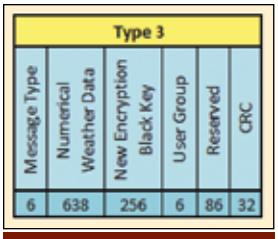

FIGURE 25 Type 3 message of the VC subframe and number of required bits

Subframe	Coding Scheme Used	Coding Rate
CED	LDPC (584,1168)	1/2
VC	LDPC (1024,1280)	4/5

TABLE 5. Coding schemes for CED and VC subframes

at 100 sps. A waiting time of around 50 seconds is expected.

Second, for the SPR-C, all weather information on a global scale is grouped into about 100 granules. Any user on the Earth receives the corrections for an area of about 9,000 kilometers diameter within eight consequent frames. According to the chosen transmission rate, a latency of about 8x50=400 seconds is expected for reaching the so-called objective performance. (This navigation solution includes accurate tropospheric corrections.)

Data Transmission Rates. The data for the two C-band services should be transmitted at the following rates: the PRS-C service at 100 symbols per second (sps) and the SPR-C service at 50 sps.

These numbers are not limited by the data demodulation itself. In fact, some margin still remains for increasing the data transmission rates and still achieve the required BER performance.

The main motivations for keeping the data rates to these values are due to the proposed code lengths, which allow a better acquisition performance (longer integration time and, therefore, lower C/N_0 requirements) as well as a better cross-correlation performance.

Tropo Delay Corrections in the Nav Message

GNSS positioning requires tropospheric delays to be mitigated using a suitable correction model. Broadcast of these corrections is proposed for the C-band services.

Often, so-called "blind" models are used such as the RTCA MOPS. These models are also fore-seen for Galileo. Such models are a kind of climatological database, that is, they employ look-up tables to figure out typical values describing the atmosphere at a certain location. The hydrostatic and the wet delay — the two components we normally have to distinguish — can then be approximated without any knowledge of *in situ* measurements.

Of course, such models are suitable to describe the typical expected delay under ordinary conditions but will fail as soon as unusual conditions are present. Comparisons with GPS-derived total zenith path delays over several years (carried out in an ESA study in the framework of the Galileo testbed V1) revealed an RMS in the range of about 5 centimeters in zenith direction under ordinary conditions (which map to approximately 50 centimeters at an elevation of five degrees), but residuals will tend to easily reach 1.5 to 2.5 decimeters under "unusual" conditions (which map to 1.5 to 2.5 metres at 5 degrees elevation).

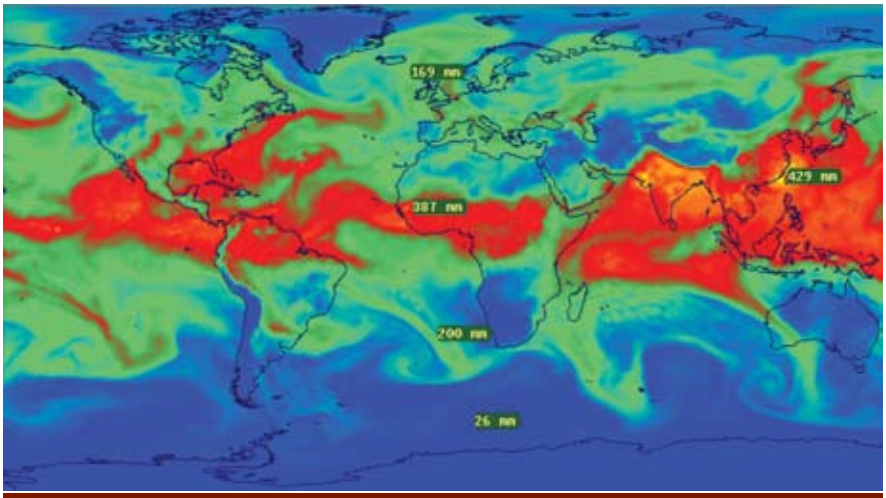

FIGURE 26 Grid of zenith wet delays (surface) as seen on July 28, 2008, at 12:00 UTC; values in units of millimeters.

The idea for improving the performance of these models is to retrieve tropospheric delay corrections from numerical weather fields, resample these data on a grid suitable for the broadcast message format, and thereby supply a more precise compensation of this error component. Initial studies on the use of such numerical weather model data indicate an accuracy in the range of 1.5 centimeters in the mid-latitudes.

Representing Tropospheric Corrections. A two-dimensional (2D) representation of the needed delay quantities and vertical modelling functions is used to reduce the amount of data to be transferred to the user and to simplify the computations.

Numerical weather fields are 3D files, and we need to integrate the refractivity profile in order to obtain those values required to compensate for the tropospheric delays in GNSS positioning. In contrast, all needed quantities will be given on a 2D grid here.

The ZHD is the largest part (often 75–90 percent of the total tropospheric delay) and can be precisely determined if pressure measurements are available at the height of the user antenna. Consequently, the quantities

$p(h)$: total pressure at a common reference height h (e.g., sea level)

q_P: pressure scale height for vertical reduction at the user height

will be needed.

Conversion from pressure to zenith hydrostatic delay is accomplished with the well-known Saastamoinen model which is internationally accepted and of high accuracy. Vertical reduction is carried out using an exponential function that relates the pressure at reference height h to any height of a receiver h_{USER} with help from the pressure scale height. Several precise mapping functions are available to project the zenith delay into a slant direction.

The ZWD component is difficult to model using surface measurements. For this reason, vertical profile integration of wet refractivity will be carried out using the 3D numerical weather fields first. The zenith wet delay will be directly given on the correction grid:

$ZWD(h)$: zenith wet delay at a common reference height h

q_{ZWD}: ZWD scale height, exponential trend for vertical reduction.

Similar to the treatment of the hydrostatic component, vertical reduc-

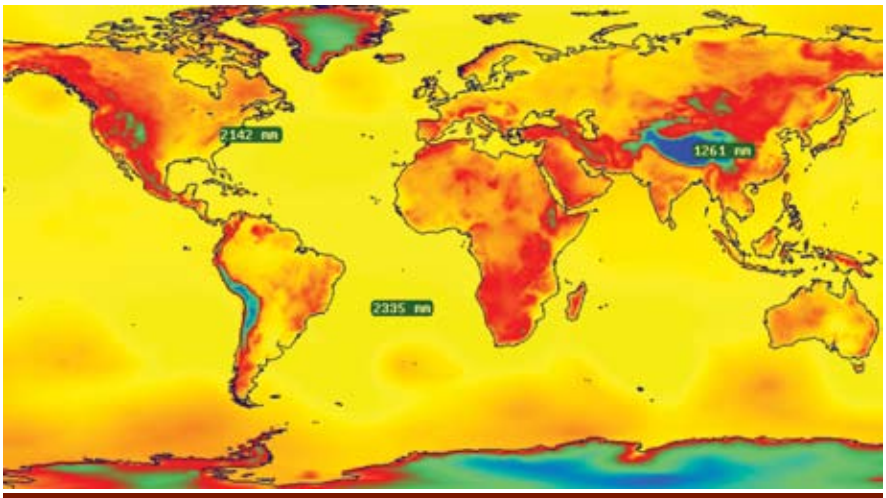

FIGURE 27 Grid of pressure/zenith hydrostatic delay as seen on July 28, 2008, at 12:00 UTC; values in millimeters.

tion can be carried out us-ing an exponential trend function $ZWD(h_{USER}) = ZWD(h)\exp(-h/q_{ZWD})$, but the scale height will be significantly different from that employed to reduce the pressure data.

The original output resolution of global numerical weather models is currently in the range of 0.5 to 1.0 degrees. This amount of data cannot be handled in a broadcast message data stream. Hence, these grids are resampled to a lower resolution supplying smoothed values on a coarser grid.

The spatial (horizontal) resolution of the tropospheric grids differs because the spatial correlation of pressure is substantially larger than that for the zenith wet delay. This fact is illustrated in **Figure 26** (ZWD) versus **Figure 27** (ZHD). In the figures, the hydrostatic component has a much higher correlation length (particularly visible over the oceans where the effect of topographic height variations cannot be seen in the selected color scale).

The following grid resolution is suggested:

ZWD, qZWD:	3° x 3°
p, qp:	6° x 6°

These grid sizes are a trade-off between the desired accuracy and the data value to be transferred to the user. They are based on an error analysis that takes into consideration the accuracy requirements as specified for the various C-band services.

Encapsulation into Broadcast Message. Transmitting a global 3 x 3-degree data grid in the navigation message will not be possible as a single data package containing all grid points. Instead, the global grid is divided into sub-grids (granules).

Figure 28 portrays such a granule with 3 x 3-degree grid containing wet delay data. In addition, hydrostatic data will be put on a 6 x 6-degree grid (blue dots). Each granule has 5 x 5 = 25 grid points. An efficient distribution scheme is to be employed for the individual satellites that will allow the efficient broadcast of the various granules relevant to the user at a particular location in a minimum of time.

Data Bits. The data to be transmitted comprise some header information (e.g., the granule identifier) and the data grid itself. The data can be reduced by typical average values in order to minimize the number of bits as efficiently as possible. In fact, it will be possible to employ the standard ("blind") Galileo tropospheric correction model for the data reduction of pressure and zenith wet delay.

The difference between the actual quantity and the blind model is the value to be transmitted.

This method is particularly useful for the pressure data, as can be seen in **Figure 29**.

Quantity	Typical range (global grid)	Number of bits
ZWD	256 mm	8
q_{ZWD}	0.5 - 5.0 km	9
p	60 hPa	6
q_p	6 - 17 km	10

TABLE 6. Expected data ranges and number of bits for a grid point

Table 6 illustrates expected data ranges and the resulting number of bit reserved for data trans-mission.

Optimization. A number of optimization issues need to be taken into consideration to reduce the data load to an acceptable minimum. Polar regions, for instance, have low temperatures and relatively small temperature variations. This means that the zenith wet delay will be by far less variable than in the tropics. For this reason, the grid resolution could be coarser in these regions.

Similarly, ocean surfaces might not be of large interest for a precision positioning service. Con-sequently, a land-sea-mask is foreseen and data over oceans can either be skipped or submitted on a coarser grid. Different data representation schemes, such as spherical harmonic coefficients, could be employed (but may be incompatible with the granule fragmentation concept). Finally, the data sections can be transmitted as compressed messages (not studied here in detail).

Integration of Rain-Rate Information. We have only dealt with the problem

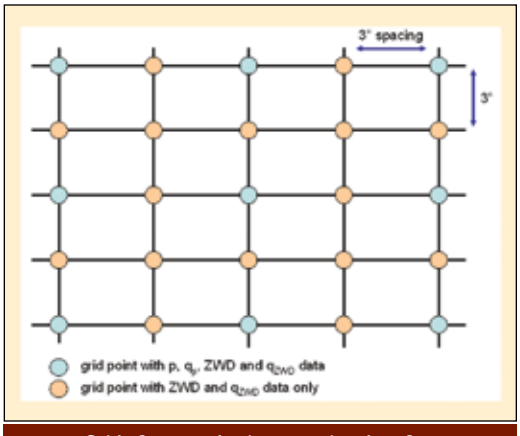

FIGURE 28 Grid of tropospheric correction data for one granule (sub-grid) with pressure (i.e., hydrostatic delay-related quantities) data available at blue dots in addition to wet delay-related quantities.

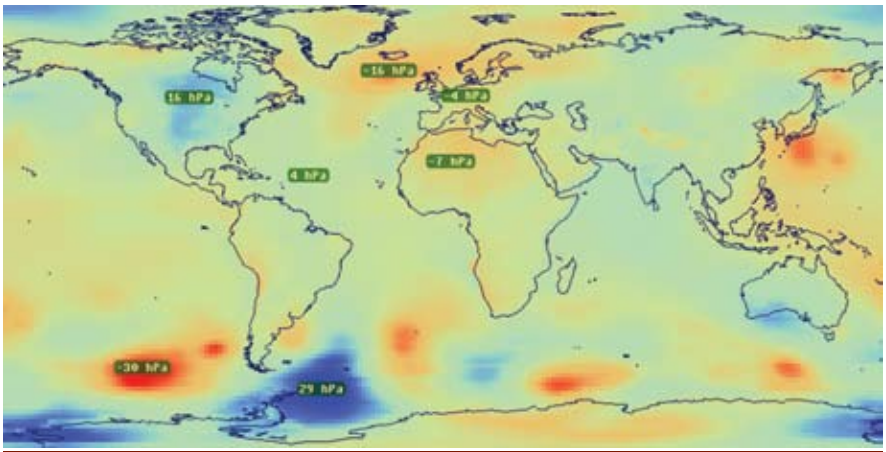

FIGURE 29 Grid of pressure/zenith hydrostatic delay as seen on July 28, 2008, at 12:00 UTC; values in millimeters.

of tropospheric delay compensation so far. Other value-added data could also be interesting for a C-band GNSS positioning service.

This is particularly true for rain-rate information, because rainfall attentuation is substantially stronger in C-band than in L-band. For this reason, such pieces of information can be vital for users in tracing signal reception problems and similar phenomena.

Incorporation of such information into the navigation message would be possible. Up to five data bits would need to be made available. Rain-rate information should be transmitted on the fine grid (3 x 3 degrees), because rain is often a local phenomenon (convection cells) and thus will likely require the highest resolution grid available.

User Terminal Critical Technologies

The C-band project also sought to identify critical technologies that would be needed to design and build user equipment capable operating with C-band in a future GNSS constellation. In the following sections, we will discuss the most important of these technologies, their significance for C-band receiver operation, their availability and state of the art, and other relevant aspects.

Beam-Forming Antenna. Compared to L-band, in order to provide the necessary signal strength for user equipment on the ground, the RF power of the C-band transmitter should be higher. However, this can cause problems in the satellite, particularly in terms of power supply and interference (especially to the Galileo uplink).

One solution to reduce this transmit power requirement would be to use a beam-forming antenna in user terminals — a quite imaginable prospect for handheld receivers. A possible further advantage of the beam-forming technique would be improved resistance to jammers. Fixed beams or phased arrays with variable beams could be used, depending on the needs of the services.

Using a phased array antenna could be especially beneficial for PRS-C services, where jamming is a hot issue. Nulling algorithms could also be incorporated into the receiver design in order to reduce strong jamming signals.

The problem of minimizing TTFF and the receiver's processing power consumption is even more complicated than the direct long-code acquisition of the C-band signal.

Because a user terminal needs to access signals from multiple satellites, it would have to have a multi-target phased-array antenna. This means that the receiver design would need to include a dedicated weighting network for each satellite.

In principle the weighting networks could be implemented at RF, IF, or baseband. From an interferer cancellation point of view, an RF weighting network would be preferable, because it would only require increased linearity for the low noise amplifier (LNA) and the weighting network (all stages in front of and including the weighting network). However, this RF solution would be expensive and bulky.

A more attractive approach would be to put the beam-forming network into the digital domain (IF or baseband). In this case the whole front-end chain has to fulfill increased linearity requirements in order to overcome the fact that a receiver is significantly disturbed by intermodulation products falling into the receive band.

Use of a phased array introduces similar considerations as for a fixed-beam array. The individual weighting networks must track the movements of the receiver and the satellites in order to maintain the nulling of the interferer.

Many algorithms are available in the literature to address such tasks. However, the phase center of the various beams will cause problems, especially when nulling is performed. Producing a null in the beam pattern will cause a phase jump between signals entering the beam in directions right and left from the null.

Low Noise Amplifier. The LNA in a GNSS receiver front-end has two primary performance aspects: the noise figure, which mainly determines the sensitivity of the receiver, and the linearity of the LNA, which determines the strength and effect of interferers whose intermodulation products are entering the receive band.

For example, two wireless local area network (WLAN) signals at 5250 MHz and 5290 MHz generate third-order intermodulation products at 5010 MHz and 5430 MHz. The product at 5010MHz falls into the receive band.

The only way to reduce these out of band interferers and their intermodulation products would be a narrow RF filter in front of the LNA. Such filters, however, tend to be either bulky and costly

(waveguide filter) or lossy, which deteriorates the noise figure of the LNA. So, use of an LNA with good linearity even at high input signal levels is desirable. Of course, good linearity usually comes along with higher power consumption. Currently, some discrete LNAs are already available for the C-band.

In the C-band the manufacturers offering C-band LNAs are more dedicated to microwave components. This can be expected to change in the next years due to the WLAN applications that are driving C-Band technology.

RF Mixer and Filter. The RF mixer is important with respect to the linearity of the system. In our work, we identified several examples from various manufacturers of passive double- or triple-balanced mixers with high linearity for discrete C-band mixers.

Most of today's C-band mixers are based on gallium arsenide (GaAs) technology, but some of them use a complementary metal oxide semiconductor (CMOS) technology capable of operating up to 6 GHz. The linearity of these passive mixers depends on the local oscillator drive level. High linearity requires high drive levels — up to 20 dBm. Again, this increases power consumption but at levels similar for both L-band and C-band.

Technologies for RF filters in C-band range from waveguide cavity filters to ceramic filters. Cheap filters in C-band are already available due to WLAN applications. The performance of such filters is not as high as with cavity filter types, but reasonable for the purpose of receiver design.

Clock Oscillator. Clock quality is an important performance parameter for high-quality receivers. A precise clock reduces the noise of the oscillators and allows for narrower loop filters in low dynamic scenarios, thereby reducing the measurement noise. The receiver clock may also be synchronized to the system time after a longer loss of the signal, dramatically reducing reacquisition times.

A precise clock is also essential for integrating the signal over a long integration time interval, as is needed for low C/N_0. Currently, precise atomic clocks are expensive, large, (rubidium clocks about 200–300 cubic centimeters) and consume much power (up to 10 watts). With the reduced size, price, and power consumption expected in the future, however, manufacturers will be able to incorporate atomic clocks into their receivers.

An alternative to the temperature controlled crystal oscillator (TCXO) could be the microcomputer controlled crystal oscillator (MCXO). The price of the latter is quite high today, but the technology is based on a crystal oscillator with some licensed electronics.

The main idea for improvement in this area is to design a dual-mode oscillator that uses the quartz in its fundamental mode and in its third overtone. The frequency of the third overtone is higher than that of the fundamental mode by approximately a factor of three — but not exactly. A small temperature-dependent difference exists that can be estimated by the MCXO electronics, and the oscillator output frequency then corrected accordingly.

As use of such a technology becomes more widespread, the price could be expected to fall into a region comparable to TCXOs.

Integrated Front-End. An integrated front-end would be especially attractive for antenna array applications, where more than one front-end section is necessary. In the L-band highly integrated front-ends are available in a commercial market, typically within 5x5 millimeters size and consume about 40 milliwatts of power. Complete one-chip solutions including processing are also available.

We can also expect a similar solution for C-band. In the field of WLAN applications, multiple C-band RF front-ends are already integrated for the WLAN MIMO standard 802.11n. The performance of such available integrated solutions will be worse than an optimized discrete solution, but progress in semiconductor technology will reduce this difference. The power consumption of such an integrated solution will be significantly less than for a discrete front-end.

Massive Parallel Correlator Technology. The number of effective correlators that can be integrated into a single chip should be an essential critical technology to acquire a direct long-code acquisition of the proposed C-band signals (or codes). Long codes need long integration times and high requirements on Doppler accuracy.

Signal acquisition time may be reduced by massive parallelization of correlations, achieved by integrating a high number of hardware correlators onto a single chip, possibly in combination with other methods. The corresponding hardware requirements have to be taken into account (for example, fast Fourier transform, circular convolution, and so forth).

Signal acquisition time may be reduced by massive parallelization of correlations, integrating a high number of hardware correlators onto a single chip.

As is well understood in the GNSS community, the problem of acquiring and tracking GNSS signals involves a two-dimensional search in Doppler and code delay. In modern all-in-view receivers with multiple correlators per receiver channel, each channel can have different Doppler frequencies and code delays in order to reduce the acquisition time (TTFF).

The problem of minimizing TTFF and the receiver's processing power consumption is even more complicated than the direct long-code acquisition of the C-band signal. Therefore, receiver design should consider a fast acquisition engine that might be based on a massively parallel array of correlators.

Combined C-/L-Band Tracking. First of all, in order to process L- and C-band signals simultaneously, both signals must be transmitted from the same satellites without any clock offset. The dominant error source of single-frequency users is due to the ionosphere, which is inversely proportional to frequency squared.

A key point of combined signal pro-

cessing of L- and C-band is to combine a common part of ionospheric propagation error between L-band and C-band efficiently. Fortunately, the ionospheric error of a C-band receiver is 3.2 times smaller than that of the L1-band receiver. Ionospheric scintillation may reduce the accuracy of a signal-tracking loop and cannot be compensated in a single-frequency receiver. The use of L- and C-band frequencies together makes it easier to correct ionospheric errors sufficiently.

A signal-tracking Kalman filter in a local signal channel simultaneously handles the combined code/carrier tracking of a single- or dual-band (or higher) signal with appropriate ionospheric delay estimation. Integer ambiguities can be included in the state vector of the signal-tracking loops and also calculated more easily by combining L- and C-band carrier phases (e.g., widelane or narrowlane).

After integer ambiguities resolved, the state vector of signal tracking loop contains only signal parameters —for example, code delay, carrier phase, Doppler frequency, and so forth — that need to be estimated.

SoC-Type INS-Aided Tracking. Over the years the integration of GNSS and inertial measurement unit (IMU) technologies has advanced from the system level to deep inside the software/hardware level. Today, a one-chip solution in single-die GNSS/IMU, including all digital signal processing components and self-alignment functionalities, is even possible even with digital technology.

Moreover, many optimistically envision the possible implementation of a low-cost, system-on-chip (SoC) level GNSS/IMU in the near future. Such an integration would consist of a single (or multiple) die on a single chip that includes all systems, such as a GNSS receiver and IMU as well as navigation/control processor blocks.

However, the SoC-type micro-electrical-mechanical-system (SoC-MEMS) integration has been considered as the next milestone in the MEMS research area. In the past, MEMS research has mainly focused on physics level and component-level designs. This has made distinct MEMS-IMU sensors affordable for a lot of applications.

Nowadays, the research effort has gradually migrated from components design to systems design, thus extending the operational performance into the SoC field for achieving better system performance and more effective cost reduction.

Unfortunately, up to now it seems that integrating a MEMS structure and a digital processing part into a single die would be problematic due to decoupling of CMOS and the MEMS structure. Therefore, only a system-in-a package (SiP) type product is now available, which means two individual dies integrated into a single package (i.e., a chip).

The SoC-type micro-electrical-mechanical-system (SoC-MEMS) integration has been considered as the next milestone in the MEMS research area.

Currently SoC MEMS is implemented with field programmable gate arrays (FPGAs) because of their flexibility and easy configurability that make it possible to implement all components into a single system. This type of system provides a platform that simplifies implementation of any type of digital hardware solution in a short development cycle. As a result, it is really efficient for a low production volume.

The main SoC-MEMS architecture is divided into two components: a sensor cube and the signal processing/communication interface circuitry. The sensor cube has the whole set of sensors and sends all captured information to the FPGA, which includes a signal processing part in which the received data are stored for later treatment.

A lot of architectures have been proposed for GNSS/IMU integrations. Among these the deeply coupled method is known as the most advanced technique. The main advantage of this technique is that the carrier tracking loop bandwidth can be significantly reduced as the IMU Doppler-aiding removes most of user dynamics from the signal-tracking loop. This improves the quality of the measurements and the anti-jamming properties of GNSS receivers.

The efficiency of this integration method depends on the quality of the Doppler estimates derived from the IMU; therefore, there is an upper limit of coherent integration time.

The RF front-end part of GNSS receiver block might be expected to be implemented in a separate single die for the same reason as with SoC MEMS: the decoupling problem of CMOS and the analog part. For example, integrating the high-frequency RF part together with the digital part in a single die has been difficult up till now. Using an SiP approach, all analog parts and the digital signal processing portion including microprocessors and memory (RAM and ROM) can be integrated into a single package.

Multi-Bit ADC. A sampling number higher than the usual one or two bits is desirable in C-band user equipment due to the continuous wave form property of the proposed GMSK signals, the constraints in the C/N_0, and the high performance requirements for the services.

However, the main driver for multi-bit sampling is not so much to reduce the quantization loss. Rather a higher sampling bit number can help cope with high dynamics in terms of the received incoming signal strength. It can also help avoid a saturation of the analog-to-digital converter (ADC) due to a jammer, enabling an active processing of the jamming signal. Multi-bit conversion results in more processing power being needed in the digital part of the receiver.

In addition to the items discussed here, many other critical technologies — such as power consumption, form factor, board, processors, and memory — were identified for the early development of C-band navigation systems.

Conclusions

A C-band signal plan was designed to fulfil the high-level requirements for

both identified services, namely the SPR-C and PRS-C. The effort focused on signal modulation schemes to comply with the stringent requirements on spectrum confinement set out to ensure compatibility with other services, according to ITU regulations, with the neighboring bands (e.g., radio-astronomy, uplink receiver, and MLS) as well as to protect the Galileo uplink receiver.

As a result, GMSK (with BT=0.3) modulated both on I and Q channels was selected. Based on an extensive signal performance analysis together with user terminal aspects, this modulation scheme was further optimized for maximum bandwidth occupation and spectral separation between the two identified services. Detailed signal parameters such as chip rate, chip length, and so on were designed to satisfy the requirement that C-band navigation services shall be competitive with current or planned L-band services.

Acknowledgements

Authors Note: It is highly remarked that this column is based upon a C-band GNSS study being conducted within the European Space Agency (ESA) GNSS Evolution Program. Please note that the views expressed in the following reflect solely the opinions of the authors and do not represent those of ESA.

Additional Resources

[1] Ávila-Rodríguez, J. A. (2008), and S. Wallner, J. H. Won, B. Eissfeller, A. Schmitz-Peiffer, J.-J. Floch, E. Colzi and J.-L. Gerner, "Study on a Galileo Signal and Service Plan for C-band", *Proceedings of ION GNSS 2008*, Savannah, Georgia, USA

[2] Irsigler, M. (2004), and G. W. Hein, and A. Schmitz-Peiffer, "Use of C-Band Frequencies for Satellite Navigation: Benefits and Drawbacks," *GPS Solutions,* Wiley Periodics Inc., Volume 8, Number 3, 2004

[3] ITU Regulations, www.itu.int/pub/R-REG-RR/en

[4] Schmitz-Peiffer, A. (2008), and D. Felbach, F. Soualle, R. King, S. Paus, A. Fernandez, R. Jorgensen, B. Eissfeller, J. Á. Ávila-Rodríguez, S. Wallner, T. Pany, J. H. Won, M. Anghileri, B. Lankl, and E. Colzi, "Assessment on the Use of C-Band for GNSS within the European GNSS Evolution Programme," *Proceedings of ION GNSS 2008*, Savannah, Georgia, USA.

[5] Schmitz-Peiffer, A. (2009), and L. Stopfkuchen, J. J. Floch, A. Fernandez, R. Jorgensen, B. Eissfeller, J. Á. Ávila-Rodríguez, S. Wallner, J. H. Won, M. Anghileri, B. Lankl, T. Schüler, O. Balbach, and E. Colzi, "Architecture for a Future C-band/L-band GNSS Mission - Part 1: C-band Services, Space- and Ground Segment, Overall Performance," *Inside GNSS* magazine, May/June 2009.

[6] Won, J. H. (2008), and B. Eissfeller, B. Lankl, A. Schmitz-Peiffer, and E. Colzi, "C-Band User Terminal Concepts and Acquisition Performance Analysis for European GNSS Evolution Programme," *Proceedings of ION GNSS 2008*, Savannah, Georgia, USA

[7] Won, J. H. (2008a), and J. Á. Ávila-Rodríguez, S. Wallner, B. Eissfeller, J.-J. Floch, A. Schmitz-Peiffer, and E. Colzi, "C-Band User Terminal Aspect for Bandwidth Efficient Modulation Schemes in European GNSS Evolution Programme," International Symposium on GPS/GNSS 2008, Tokyo, Japan

[8] Won, J. H. (2008b), and B. Eissfeller, A. Schmitz-Peiffer, and E. Colzi, "C-Band User Terminal Tracking Loop Stability Analysis for European GNSS Evolution Programme," *Proceedings of ION GNSS 2008*, Savannah, Georgia, USA

[9] Won, J. H. (2008), and B. Eissfeller, A. Schmitz-Peiffer, and E. Colzi, "C-Band User Terminal RFI Effect Analysis for European GNSS Evolution Programme," *Proceedings of the Fifth ESA NAVITEC-2008,* Noordwijk, The Netherlands

Authors

"Working Papers" explore the technical and scientific themes that underpin GNSS programs and applications. This regular column is coordinated by **PROF. DR.-ING. GÜNTER HEIN.**

Prof. Dr.-Ing. Hein is head of Galileo Operations and Evolution for the European Space Agency. He is a member of the European Commission's Galileo Signal Task Force and organizer of the annual Munich Satellite Navigation Summit. He has been a full professor and director of the Institute of Geodesy and Navigation at the University of the Federal Armed Forces Munich (University FAF Munich) since 1983. In 2002, he received the United States Institute of Navigation Johannes Kepler Award for sustained and significant contributions to the development of satellite navigation. Hein received his Dipl.-Ing and Dr.-Ing. degrees in geodesy from the University of Darmstadt, Germany. Contact Prof. Dr.-Ing. Hein at <Guenter.Hein@unibw-muenchen.de>.

José-Ángel Ávila-Rodríguez received his PhD in signal design at the Institute of Geodesy and Navigation at the University of FAF Munich. He is

responsible for research activities on GNSS signals, including BOC, BCS, and MBCS modulations. Avila-Rodriguez is one of the CBOC inventors. He is involved in the Galileo program, where he supports ESA, the European Commission, and the Galileo Supervisory Authority (GSA), through the Galileo Signal Task Force. He studied at the Technical Universities of Madrid, Spain, and Vienna, Austria, and has a M.S. in electrical engineering.

Jong-Hoon Won received his Ph.D. in control and instrumentation engineering at Ajou University, Suwon, Korea. His thesis was on signal processing, simulation, and navigation algorithms for software-based GPS receivers. Currently he is working at the Institute of Geodesy and Navigation at the Federal Armed Forces (FAF) University Munich, Germany. His current research activities are software GNSS receivers, GNSS/INS coupling systems, and user terminals.

Stefan Wallner studied at the Technical University of Munich and graduated with a Diploma in techno-mathematics. He is now research associate at the Institute of Geodesy and Navigation at the University of the Federal Armed Forces Germany in Munich. His main topics of interests can be denoted as the spreading codes, the signal structure of Galileo together with radio frequency compatibility of GNSS.

Marco Anghileri is a research associate and Ph.D. candidate at the Institute of Geodesy and Navigation at the University FAF Munich. He studied at the Politecnico di Milano, Italy, and at the Technical University Munich, Germany and has an M.Sc. in telecommunication engineering. His scientific research work focuses on GNSS signal structure and on signal processing algorithms for GNSS receivers.

Bernd Eissfeller is full professor and director of the Institute of Geodesy and Navigation at the University FAF Munich. He is responsible for teaching and research in the field of navigation and signal processing. Until the end of 1993 he worked in industry as a project manager on the development of GPS/INS navigation systems. From 1994 to 2000 Eissfeller was

head of the GNSS Laboratory at University FAF Munich. He is author of more than 215 scientific and technical papers.

Berthold Lankl received his Dipl.-Ing. from the Technical University Munich and his Dr.-Ing. from the University FAF Munich. He has 20 years experience in the development of radio relay systems at several positions in the industry. Since 2003 he is a professor of communications engineering at the University FAF Munich.

Torben Schüler received his diploma in geodesy and cartography from the University of Hannover in 1998. He later joined the Institute of Geodesy and Navigation (IGN), University FAF Munich, as a research associate, where he earned a doctorate and received the habilitation in geodesy and navigation. Schüler is currently head of the GNSS/INS laboratory at IGN. His major research work is focused on precise GPS/Galileo positioning, including atmospheric delay modeling.

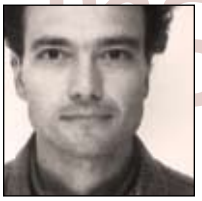

Oliver Balbach joined IFEN GmbH in 2006 where he is involved in the Galileo testbed project GATE and in projects concerning the development of GNSS receivers. He received his Diploma in electrical engineering from the Technical University München and has worked as a patent examiner at the German Patent Office and as research associate at the University FAF Munich IGN.

Andreas Schmitz-Peiffer received his Master's and Ph.D. in atmospheric physics at Kiel University, Germany. He has 19 years of experience in system engineering and project management in earth observation and navigation. Since 2000 he has been working at EADS Astrium GmbH as project manager in the Galileo program, where he is presently leading the C-band study and an indoor navigation project.

Jean-Jacques Floch was graduated with a Diplom-Ingenieur in electronics and telecommunication at the Institut Supérieur Electronique Numérique in France. He has worked in the area of mobile communications for several years. Since 2002 he has been working in the field of navigation satellites as system engineer at EADS Astrium. His work is mainly focused on Galileo signal design at the system level and evaluation of performances and robustness of Galileo signals.

Lars Stopfkuchen received his Diploma at the University of Cooperative Education Ravensburg, Germany in communications engineering. He joined EADS Astrium GmbH in 2003 as design engineer for FPGA and ASIC developments and participated in GIOVE-B and other ESA projects. Currently he conducts system engineering tasks for electronics subsystems and is responsible within the C-band study for the navigation payload design.

Dr. Dirk Felbach received his Ph.D. in 2001 from the Technical University Munich in Radio Frequency Engineering. Since then he is with Astrium working as a Systems Engineer and Project Manager on navigation payload equipment for time and signal generation.

Antonio Fernández received his M.S. degree in aeronautical engineering from the Polytechnic University of Madrid and an M.S. in physics from the UNED University of Spain. He has been working in the field of GNSS since 1996. Fernández co-founded DEIMOS Space in 2001, where he is currently in charge of the GNSS technologies section.

Rolf Jorgensen received his MScEE degree from the Technical University of Denmark. An antenna expert with long experience, he has been involved in the design support for development of C-band and Ku-band satellite communication payloads for ESA and INTELSAT and responsible for the antenna design in numerous other ESA projects.

Enrico Colzi, received his Ph.D. from the Technical University of Delft, The Netherlands and his M.Sc in telecommunication engineering from the University of Florence, Italy. He was with the European Space Agency (ESA), the Italian Space Agency, and the University of Florence. Currently he is working for Vega Group PLC as senior RF payload engineer in the RF Payload System Division of ESA/ESTEC. IG